3

Thermoplastic Polymer based Modified Red Mud Composites Materials

A.H. Bhat[1], H.P.S. Abdul Khalil and A. K. Banthia[2]
[1]*School of Industrial Technology, Universiti Sains Malaysia, Penang-11800,*
[2]*Materials Science Centre, Indian Institute of Technology Kharagpur-721302,*
[1]*Malaysia*
[2]*India*

1. Introduction

Soaring prices are a reminder of the essential role that affordable products play in sustainable economic growth and higher human development. Utilization of waste materials has become more pressing than ever. Red mud is accumulating at a rate of 30 million ton annually throughout the world. Under normal conditions when 1 ton of alumina is produced from bauxite, an equal amount of red mud is generated as a waste. A further aspect is their reuse as starting materials for other products (Grjotheim & Welch, 1998; Kasliwal, & Sai, 1999). Red mud has been suggested as filler for polymer reinforcement or as a cheap adsorbent for removal of toxic metals or an acid by several researchers. Chand and Hashmi, 1999, tried to improve the mechanical properties and abrasive wear properties of polymer blend filled with red mud. Pradhan et al. 1999 had reported that activated red mud as a good adsorbent was used for adsorption of phosphate or chromium. In addition, the mechanical and thermal properties of polymers are generally improved by the addition of inorganic fillers. The challenges in this area of high-performance organic–inorganic hybrid materials are to obtain significant improvements in the interfacial adhesion between the polymer matrix and the reinforcing material since the organic matrix is relatively incompatible with the inorganic phase. Generally, a better interfacial bonding will impart better properties to a polymer composite such as high modulus, strength, and stiffness (Agag et al., 2001; Jang, 1992).This reinforcement of polymer filled with inorganic material is largely dependent on the physical interfacial phenomenon between the filler and matrix. This can be determining the degree of adhesion by physical interaction, such as active functional groups, hydrogen bonding, Lewis acid–base interactions, surface energy, and crystallite faces of filler surface at the interface (Park & Kim, 2000; Park & Cho, 2000). To increase physical interaction, various surface treatment techniques are applied, such as oxidation in acid solutions, (Donnet & Bansal, 1990) dry oxidation in oxygen, (Yuan et al., 1991) anodic oxidation, (Ishikawa & Matsumoto, 2001; Park, S. J.; Kim) and plasma treatments (Dilsiz et al., 1995). Surface modification leads to development of surface functional activity on a filler surface, resulting in modification to achieve good interfacial adhesion between the reinforcement and the matrix.
In materials research, the development of polymer nanocomposites is rapidly emerging as a multidisciplinary research activity whose results could broaden the applications of

polymers to the great benefit of many different industries. The details about worldwide generation of Red Mud, country wise and region wise is shown in fig. 1.

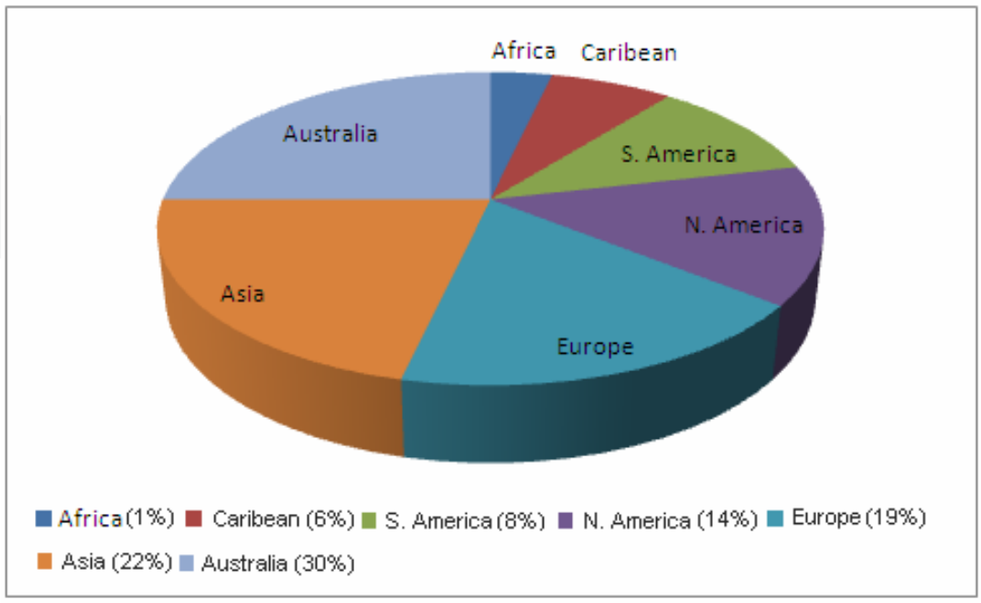

Fig. 1. Red Mud generation Continent/Region wise

The use of layered inorganic fillers has been a common practice in the plastics industry to improve the properties of thermoplastics. The effects of filler on the material properties of composite materials depend strongly on its particle size, shape, aggregate size, surface characteristics, and degree of dispersion. Polymer composites prepared in combination with an organic component as a matrix and an inorganic component as filler on the nanoscale (Huang et al., 1987; Suriyet et al., 1992; Novak & Ellsworth, 1993; Hajji et al., 1999) have additional advantages, such as the possibility of obtaining a material that has the advantages of both organic materials (e.g., light weight, flexibility, good moldability) and inorganic materials (e.g., high strength, heat stability, and chemical resistance)(Shao et al, 2003).

Low volume additions (≤5%) of nanoparticles of layered red mud provide property enhancements with respect to the neat resin that are comparable to those achieved by conventional loadings (15-40%) of traditional fillers. Red mud (nanofiller) is a major waste material obtained during the production of alumina from bauxite by the Bayer's process. It comprises of silicates and oxides of iron, aluminum, sodium, calcium and titanium, along with some other minor constituents. Based on economics as well as environmental related issues, enormous efforts have been directed worldwide towards red mud management issues i.e. of utilization, storage and disposal. Different avenues of red mud utilization are more or less known but none of them have so far proved to be economically viable or commercially feasible.

Thermoplastics have a big potential for applications in the industry as well as in construction, electrical applications and food packagings. One of the few disadvantages associated with the use of nanofillers, is their high cost. The present research work has been undertaken with an objective to explore the use of red mud as a reinforcing material as a low cost option. This is due to the fact that red mud alone contains all these reinforcement elements and is plentifully available.

In mechanical reinforcement major issues are the homogeneous dispersion of nanofillers in the polymeric matrix and the developments of chemical bonding or strong interaction at the nanofiller-matrix interface. In this study we have used acid modified and organically modified red mud for better homogeneous dispersion as well as enhanced material properties. The focus of this research was to experimentally characterize the two polymer nanocomposite systems and investigate the role of modification of filler in their behavior. Modified Red mud nanoparticles were dispersed in poly (vinyl alcohol) (PVA) and poly hydroxy ether of bisphenol-A (Ph) matrices.

The conventional solvent casting technique was employed to generate polymer nanocomposites. Red mud was treated with boric acid and phosphomolybdic acid to develop the acidic functional groups or active oxygen, resulting in the better dispersion of the red mud into the polymer matrices. Red mud was also organically modified with the oligomers of aniline formaldehyde, for better interaction between the filler and the polymer matrices. The particle size of the modified red mud was determined by field emission scanning electron microscopy (FESEM). The as-synthesized composite films were typically characterized by FTIR spectroscopy and X-Ray Diffraction. The morphological image of the composite materials was studied by scanning electron microscopy (SEM) and the dispersion of the modified fillers within the matrix was studied by transmission electron microscopy (TEM).The thermal properties measured by thermogravimetric analysis (TGA) showed enhanced thermal stability of a series of composite materials. The differential scanning calorimetry (DSC) showed increase in glass transition temperature and crystallization of the composite films.

The physical topography of the composite materials was studied by Atomic Force Microscopy (AFM).

Polyvinyl alcohol (PVA) is cornmercially available in dry granular or powdered form. It is a water-soluble and fully biodegradable polymer (Chen et al., 2000; Bachtsi & Kiparissides, 1996). PVA is having planar zigzag structure like polyethylene (Horii et al., 1992). All PVA grades are readily soluble in water. As a hydrophilic polymer, PVA exhibits excellent water retention properties. Conditions for dissolution are governed primarily by degree of hydrolysis, but they are influenced by other factors such as molecular weight, particle size distribution and particle crystallinity [Peppas & Merrill 1977]. Optimum solubility occurs at 87-89% hydrolysis. The partially hydrolyzed grades in this range exhibit a high degree of cold-water solubility. For total dissolution, however, they require water temperatures of about 185°F (85°C) with a hold time of 30 minutes. It is, in fact, a refinement of PVAcetate since the most common manufacturing process is to replace by hydrolysis (or alcoholysis) the acetate groups with hydroxyl groups. This is commonly achieved using the presence of catalytic quantities of alkali such as sodium hydroxide (which, since it acts only as a catalyst, should not in theory remain in the final product). The extent of hydrolysis will determine the amount of residual acetyl groups and this in turn apparently affect the viscosity characteristics.[Ray & Bousmina ,2005] PVA exists only as a polymer; a monomer has not yet been isolated, so the chemical structure is described in Fig.2.

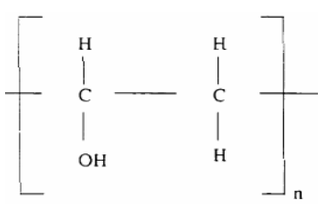

Fig. 2. Chemical formula of PVA

The PVA concentration in an aqueous solution is determined by the type of application. However, at concentrations greater than 10 wt%, the viscosity of the aqueous solution at room temperature is such that pouring becomes difficult. In addition to its solubility, PVA is also appreciated for its good mechanical properties in the dry state, resistance to common solvents, barrier effect in dry atmospheres, possibility of food contact for suitable grades, biodegradability. Some of the physical properties of PVA are as presented in table 1.

Properties	Values
Appearance	White to cream granular powder
Density	1.23-1.30 g/cm^3
Thermal stability	Gradual discoloration above 100 ^{o}C; darkens rapidly above 150 ^{o}C; rapid decomposition above 200 ^{o}C.
Coefficients of thermal expansion	7-8 x 10^{-5}/ ^{o}C
Thermal conductivity	0.2 W/m.k
Yield Stress	40-50 MPa
Elongation at break	100-200%
Melting point	230 ^{o}C for fully hydrolysed grades 180-190 for partially hydrolysed grades.
Glass transition temperature	75-85 ^{o}C

Table 1. Physical properties of PVA

PVA can be plasticized and processed by casting, dipping, injection and extrusion. (Biron, 2007).

The main engineering applications, possibly in combination with other polymers, are:

- Films for packing chemicals, fertilizers, herbicides, disinfectants, dyes, colorants, scalers, cosmetics etc.
- Release films for composite moulding.
- Solvent resistant tubes and pipes.
- Membranes for pumps carrying petroleum or chemical products

Trade names: Elvanol, Polyviol, Mowiol, Rhodoviol.

The commercial name of poly (hydroxy ether) of bisphenol A is Phenoxy, and as a thermoplastic polymer it possesses many excellent properties such as (Zhang et al., 2002)

- Good chemical stability
- Excellent matrix material for producing polymer nanocomposites
- Thermal stability
- Tractability
- Transparency

The poly (hydroxy ether of bisphenol A) (phenoxy (Ph)) has been revealed as a polymeric matrix able to intercalate in, and partially exfoliate a commercial organically modified montmorillonite. Dispersion was attributed to chemical interactions between the Ph and the inorganic clay (Fornes et al., 2004).

Poly (hydroxy ether of bisphenol A) (Ph) based polymer nanocomposites (PN) reinforced with a layered red mud with acidic and organic modifications were prepared by conventional solvent casting technique. The best dispersion occurred in the PN where the interactions between the functional groups of the polymer matrix and those of the organic substitution of the red mud appeared to be the highest. The modulus increase is an indirect but quantitative measurement of the attained dispersion level.

The structure of Poly (hydroxy ether) of bisphenol A is shown in fig.3.

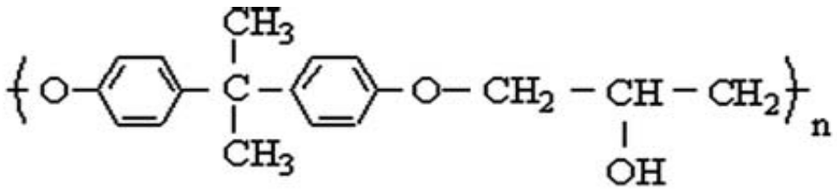

Fig. 3. Poly (hydroxy ether) of bisphenol A

2. Modification of red mud

2.1 Preparation of boric/phosphomolybdic acid modified-red mud

A known amount of raw red mud was first washed with distilled water two to three times and then dried in an oven. When the red mud dried completely; it was treated with a 5 M solution of boric acid/ phosphomolybdic acid for 24 hours. Then it was being filtered, dried, weighed and grinded in order to get its powdered form. The weight of the red mud increased by 24 %. The powder was then sieved through 53-micron mesh to remove the larger particles. The powder so obtained was fine and acidically modified. Thus, Layered silicates and double layered hydroxides, $Al_2 (OH)_7$ (AH) and $MgAl (OH)_5$ (MAH), of red mud were modified with inorganic acids. The inorganic acid modifier compatibilizes the silicate and hydroxide surface to polymer matrices and spaces the crystalline layers apart to minimize the energy needed for exfoliation process.

2.2 Preparation of organically modified-red mud

The organic modification of red mud was done by the following two steps:

i. Freshly prepared Aniline Hydrochloride is mixed with red mud with a magnetic stirrer.
ii. Formaldehyde is then added drop by drop to the mixture with intense stirring action.

The addition of aniline hydrochloride to red mud replaces the cation present in the octahedral sites of the silicate with aniline occupying the same. The formaldehyde added would form a condensation oligomer as the product with the pendent group as formaldehyde which is compatible with the polymer. The ratio of Aniline to formaldehyde is kept 1:1 so as to stop any further condensation of the aniline and formaldehyde as this could lead to the polymer blend type nanocomposite, which could have the problems associated with miscibility of polymer blends and this filler would not be universal filler for the polymer matrix. The figure 4 depicts the experimental setup for the organic modification of red mud.

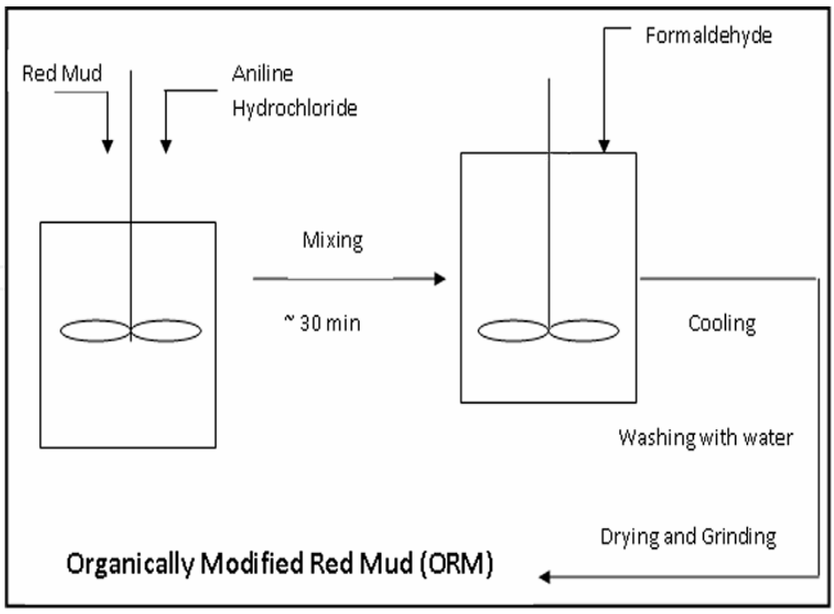

Fig. 4. Experimental setup of organic modification of red mud

2.3 Mechanism:

Figure 5 showed the mechanism and condensation reaction between substituted aniline and formaldehyde. After substitution of the metal cation, condensation reaction occurs between the substituted amine group with extra hydrogen and the formaldehyde molecule to form water as a byproduct. Thus the organic entity enters the space between the silicate layers thus providing a suitable site for binding the polymer. When this filler is mixed with the polymer, the polymer chains are attracted due to the presence of the organic species at the interlayer spaces, and thus get intercalated in between the layers, which have about nanometer size openings.

The reaction mechanism can be best depicted by the following sequence

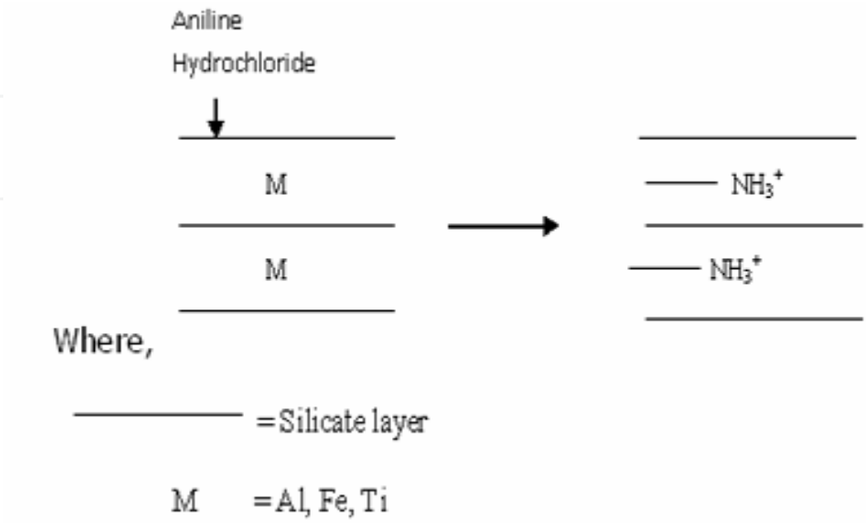

Mechanism for organic modification of red mud

Condensation reaction between substituted aniline and formaldehyde

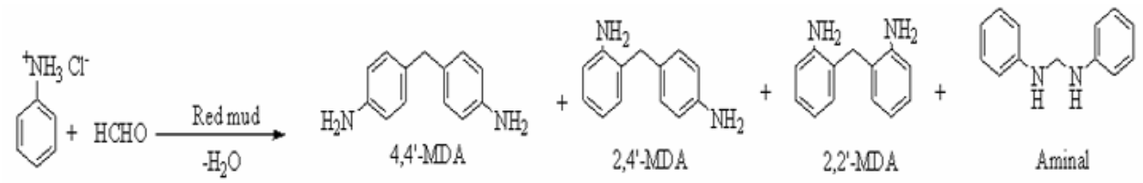

Fig. 5. Mechnaism and Condensation reaction showing Organic Modification of Red Mud

3. Experimental

3.1 Preparation of PVA-acid red mud nanocomposite materials and organically modified red mud nanocomposite materials

10% (w/v) aqueous solution of PVA was prepared by dissolving 10g of dried powdered PVA in 100ml of distilled water at a temperature of 100 ^{o}C with continuous stirring. Polymer modified red mud nanocomposite (PRM) films were made by mixing different loading percentage of acid modified red mud and organically modified red mud into the virgin PVA solution. The PVA-red mud solution thus obtained was sonicated for better dispersion and removal of any air bubble present in the solution. The solution was cast on the plane glass surface and dried at room temperature. The composition of the PRM materials was varied from 0 to 5 wt % of RM with respect to the PVA content.

3.2 Red mud loading levels

Sample index	PVA	SP1	SP2	SP3	SP4	SP5	SP6	SP7
% Loading of boric acid mod. red mud	0	0.5	1.0	1.5	2.0	3.0	4.0	5.0

Sample index	PVA	CP1	CP2	CP3	CP4	CP5	CP6	CP7
% Loading of organically mod. red mud	0	0.5	1.0	1.5	2.0	3.0	4.0	5.0

Sample index	PVA	PRM1	PRM2	PRM3	PRM4	PRM5	PRM6	PRM7
% Loading of Phosphomolybdic acid mod. red mud	0	1.0	1.5	2.0	2.5	3.0	4.0	5.0

Table 2. Sample Designation

3.3 FTIR spectroscopy

The nature of the chemical bonds in raw red mud and the modified red mud were characterized by FTIR spectroscopy. The FTIR spectra of raw red mud and acid modified red mud are shown in Fig. 5 and it clearly depicts the main characteristic peaks associated with them. The characteristic vibration band of raw red mud for hydroxyl stretching vibration (O-H) was found at 3417 cm^{-1} while for boric acid modified red mud, the hydroxyl stretching occurred at 3379 cm^{-1} and the same characteristic peak for phosphomolybdic acid was observed at 3129 cm^{-1}. A red shift in the hydroxyl stretching vibration (O-H) at 3379 cm^{-}

$^{-1}$ in the boric acid modified red mud (BRM) and 3129 cm^{-1} in the phosphomolybdic acid modified red mud (PRM) arises due to disappearance of the hydroxyl groups upon cross linking reaction with the boric acid and the phosphomolybdic acid respectively. The peak at υ = 993 cm^{-1} in case of raw red mud could be attributed to Si-O stretching vibration and the same peak for BRM and PRM were observed at 1000 cm^{-1} and 996 cm^{-1} respectively. The blue shift observed in the peak position of Si-O occurred due to the interaction of red mud with the inorganic acids.

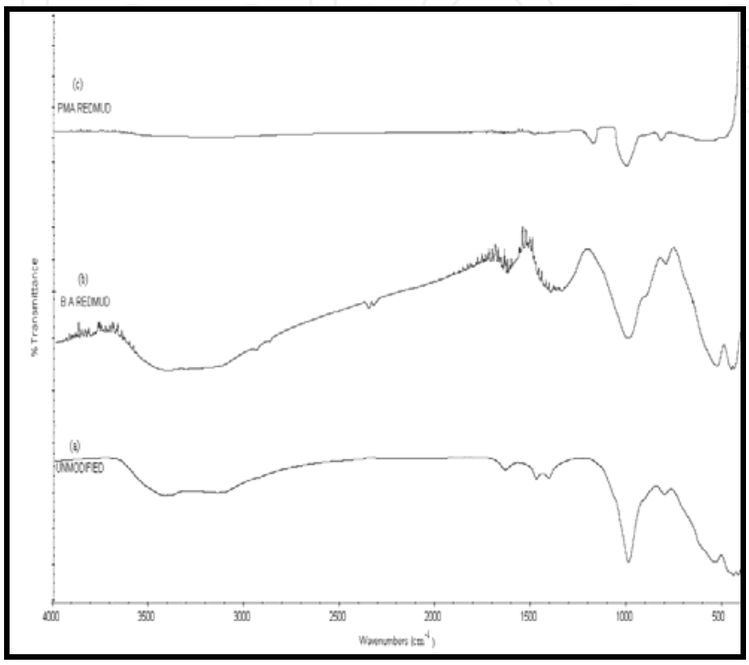

Fig. 5. FTIR Spectra of (a) Raw red mud (b) Boric acid modified red mud (BRM)
(c) Phosphomolybdic acid modified red mud (PRM)

According to the Rocchiccioli - Deltcheff et al. [80], the four absorption bands in the spectrum of pure phosphomolybdic acid (PMA) shows the typical features of Keggin anions and the peak frequencies at 1064, 961, 868, 780 cm^{-1} are assigned to the ν (P-O), ν (Mo-O_t) (O_t refers to the terminal oxygen), ν (Mo-O_c-Mo) (O_c refers to the corner oxygen) and ν (Mo-O_e-Mo) (O_e refers to the edge oxygen) respectively. All these characteristic bands of PMA are not present in the spectra of the PRM, indicating that there is specific interaction between the keggin structure and red mud.

Groups	Raw red mud (cm^{-1})	BRM (cm^{-1})	PRM (cm^{-1})
OH	3417	3379	3129
OH bend.	1636	1631	-
B-O	-	1368	-
Si-O	993	1000	996
P-O	-	-	1074
Mo-O_c-Mo			872

Table 3. Assignment of FTIR spectral bands for raw red mud and the acid modified red mud

An upward shift was observed for the ν (P-O) and ν (Mo-O_c-Mo) stretching vibrations, whereas bands ascribed to the stretching vibration ν (Mo-O_t) does not appear in the PRM.

The major vibration bands for organically modified red mud as shown in Fig. 6 occurs at OH/NH stretching (3320 cm^{-1}), NH_3^+ (1598 cm^{-1}) and Ar-N (1512 cm^{-1}). A red shift in the hydroxyl peak at 3320cm^{-1} for modified red mud arises due to the interaction of red mud platelets with the aniline hydrochloride moiety through physical interactions. The characteristic Si-O stretching vibration is not found in case of ORM due to formation of a coating of organic moiety around the silicate galleries.

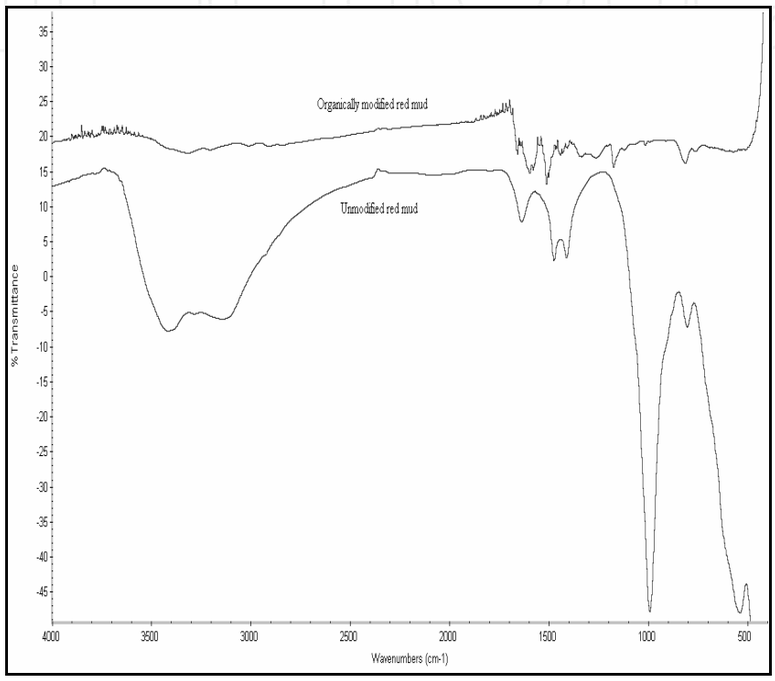

Fig. 6. FTIR Spectra of Raw red mud and organically modified red mud (ORM)

Groups	Raw red mud (cm^{-1})	ORM (cm^{-1})
OH	3417	3320
OH (bending)	1636	-
NH3+	-	1598
Ar-N	-	1512
Si-O	993	-

Table 4. Assignment of FTIR spectral bands for raw red mud and organically modified red mud

The representative FTIR spectra of the pure PVA and various polymer nanocomposite materials are shown in Fig.7.The characteristic vibration band of PVA for hydroxyl stretching vibration(O-H) having polymeric association is shown at 3292 cm^{-1}, While the alkyl stretching band of C-H is shown at 2942 cm^{-1}.The peak at υ=1736 cm^{-1} is due to C=O

stretching of saturated aliphatic esters (acetate), 1042cm^{-1}(O-H Bending), and 1424 cm^{-1} (C-H Bending).

The FTIR spectrum in Fig. 3.6 also shows the spectra associated with PRM2, SP2 and CP2. The intensity of the O-H stretching vibration peak (v = 3200-3400 cm^{-1}) decreased and peak frequency shifted from 3292 to 3250 cm^{-1}, i.e. to a lower frequency as compared to that of pure PVA. The red shift in the hydroxyl stretching frequency occurs due to the various degree of hydrogen bonding between the polymer and the filler which lengthens and weakens the O-H bond and hence lowers the vibrational frequency. Also, the peak frequency of C-H for PRM2, SP2 and CP2 occurs at 2916 cm^{-1}, 2945 cm^{-1} and 2960 cm^{-1} respectively as tabulated in Table 5.

By loading 1% ORM (CP2) in the polymer matrix, the alkyl stretching vibration of C-H increases from 2942-2960 cm^{-1} and occurs due to the interaction of polymer matrix with the organic moiety of the filler.

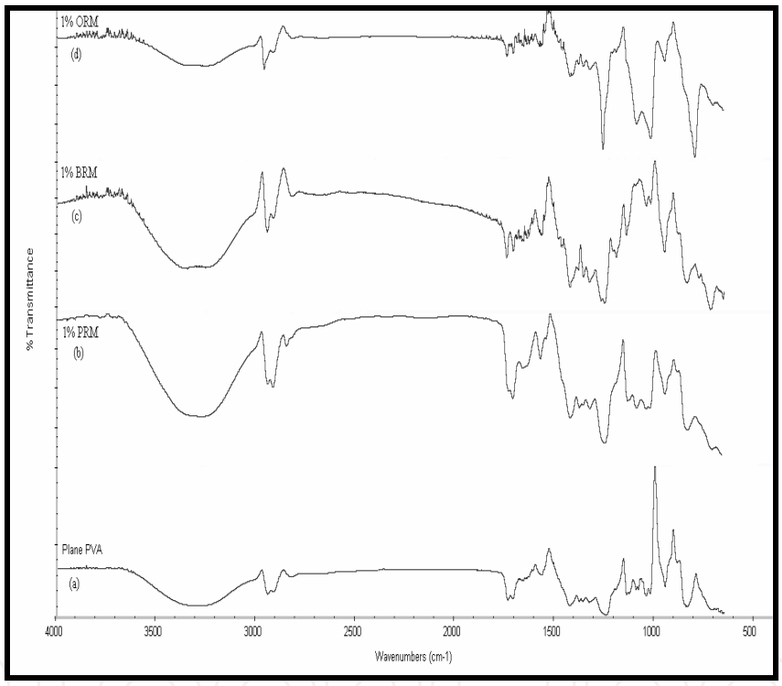

Fig. 7. FTIR Spectra of (a) Pure PVA (b) PRM2 (c) SP2 (d) CP2

Groups	PVA (cm^{-1})	PRM2 (cm^{-1})	SP2 (cm^{-1})	CP2 (cm^{-1})
OH	3292	3268	3267	3250
C-H	2942	2916	2945	2960
C=O	1736	1712	1743	1742
O-H (bending)	1042	1043	1041	1019
CH_2 (bending)	1424	1423	1424	1414

Table 5. Assignment of FTIR spectral bands for Pure PVA and the PVA/modified red mud nanocomposite membranes

The FTIR spectra in Fig. 8 shows the spectra associated with PRM4, CP4 and SP4.The intensity of the O-H stretching vibration peak (v = 3200-3400 cm^{-1}) decreased and the peak frequency shifted from 3292 in case of pure PVA to 3278 cm^{-1}, 3245 cm^{-1} and 3230 cm^{-1} for PRM4, CP4 and SP4 respectively i.e. to a lower frequency as compared to that of pure PVA. This is again due to the intermolecular hydrogen bond formation, thereby decreasing the O-H stretching frequency with the increase in the percent loading of the modified filler. The other characteristic peaks are given in table 6.

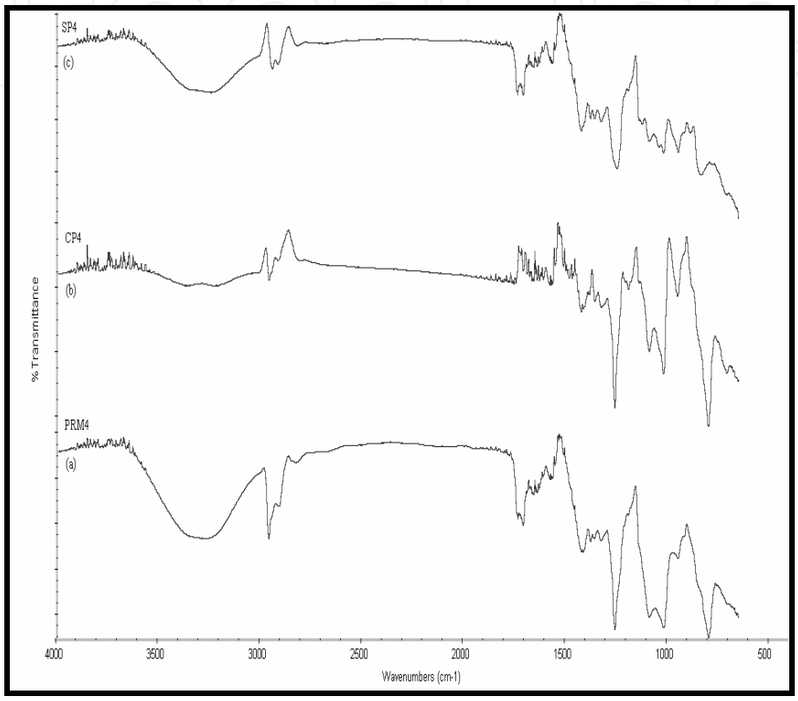

Fig. 8. FTIR Spectra of (a) PRM4 (b) CP4 (c) SP4

Groups	PRM4 (cm^{-1})	SP4	CP4
OH	3278	3245	3230
C-H	2961	2943	2959
C=O	1711	1737	1754
O-H (bending)	1020	1021	1020
CH_2 (bending)	1414	1424	1424

Table 6. Assignment of FTIR spectral bands for PVA/modified red mud nanocomposite membranes with different loading percentage of filler

3.4 X - ray diffraction study

Wide angle X-ray diffraction studies were performed on raw red mud and the modified red mud as shown in Fig. 9.

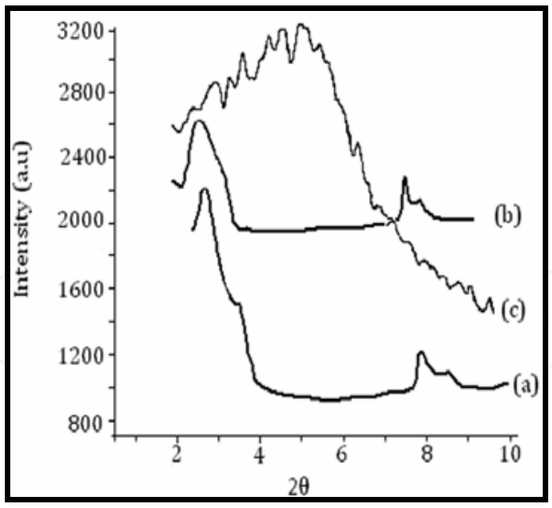

Fig. 9. Xrd pattern of (a) Raw red mud (b) Phosphomolybdic acid modified red mud (c) Organically modified red mud

The spacing, d_{001}, of the (001) basal reflections of the Raw red mud and PRM were measured and are shown in table 7. It was found that the basal spacing of the PRM is larger than the raw red mud.

Sample	2θ	d-spacing (A°)
Raw red mud	2.71	32.76
PRM	2.46	36.72

Table 7. XRD basal spacing results of raw red mud, and acid modified red mud

In the ORM, the case appears to be slightly different with the peak being lost. Thus, we could infer that the silicate layers undergo exfoliation or random dispersion at the modification stage itself. This suggests that the aniline formaldehyde type precursor have formed a coating on the partially exfoliated silicate layers leading to random dispersion thus rendering the absence of peaks in the XRD micrograph (Alexandre & Dubois, 2000).

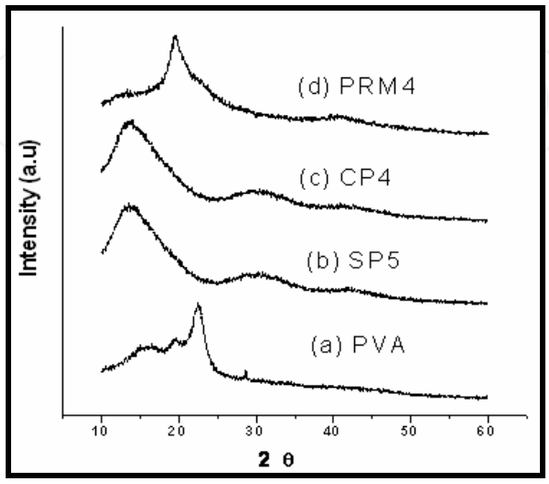

Fig. 10. X-ray Diffraction pattern of (a) PVA (b) SP5 (c) CP4 (d) PRM4 film

The XRD patterns for the Virgin PVA and the PVA nanocomposite films with different critical loading percentage of modified red mud were depicted in Fig. 10. The crystallinity of the nanocomposite membranes was found to be mainly due to PVA. The characteristic diffraction peak for pure PVA was observed at 2θ value of 22.56°. While the diffraction peak of the nanocomposite films were considerably broadened and displaced to lower 2θ values as shown in table 8, indicating reduction in the crystallinity of the nanocomposites.
The spacing, d_{001}, of the (001) basal reflections of the silicate galleries of the PVA nanocomposite films were measured as shown in table 3.9. It was found that the basal spacing for CP4 is larger than other nanocomposites materials, thereby giving evidence of more exfoliation in CP4 than the rest nanocomposites. Hence, it can be concluded that the interlayer spacing got increased by intercalation of polymer matrix. So, a lot of surface area of modified red mud is now available to the polymer for bonding.

Sample	2θ	d_{001}-spacing (A°)
SP5	13.47	6.56
CP4	13.11	6.74
PRM4	19.15	4.63

Table 8. XRD d_{001}-spacing Results

The change of crystalline behavior was further evidenced by the studies of the morphological image of as-synthesized materials. Individual silicate layers, along with two, three and four layer stacks, were found to intercalate and partially exfoliate in the PVA matrix.

3.5 SEM

On higher magnification (10,000 X) viewing of morphology of pristine PVA SP4 and SP5 type of nanocomposite films in Figure 11 (a) , (b) and (c) respectively, it was found that the morphology of polymer nanocomposite films becomes much smooth than pure PVA.

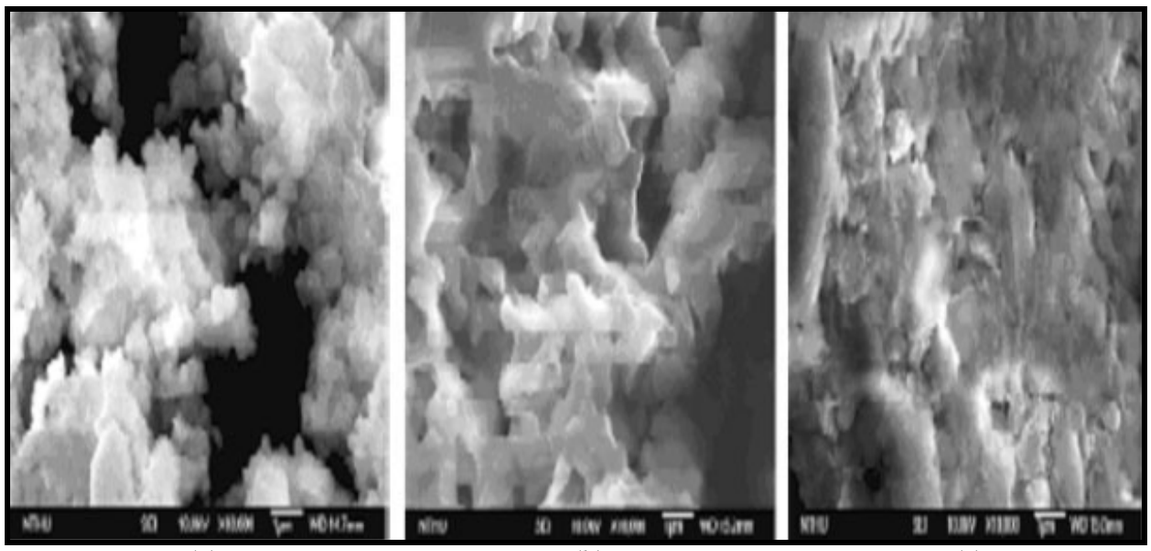

(a) (b) (c)

Fig. 11. SEM micrographs of (a) PVA (b) SP4 (c) SP5

The granules shape of PVA indicates some crystalline behavior occurring in pure polymer. The incorporation of red mud seems to destroy the orientation of semicrystalline polymer and to convert the polymer morphology approaching to amorphous state. [Bhat & Banthia, 2007] The SP5 showed much smooth morphology that is different to crystallites of PVA observation. This result is consistent with the wide-angle powder XRD patterns as described previously.

3.6 Transmission Electron Microscopy (TEM)

TEM complements XRD by observing a very small section of the material for the possibility of intercalation or exfoliation. It also provides information about the particle size and nanodispersion of particles. It however, supplies information on a very local scale. However, it is a valuable tool because it enables us to see the polymer and the filler on a nanometer scale.

The images, in Fig.12, 1 3 and Fig. 14, provide information regarding likely sizes of particles present in the matrix. Figure shows each of the polymer nanocomposite systems with critical loading of modified red mud. In Fig. 12 the silicate galleries of the organically modified red mud showed partial exfoliation and intercalation as depicted by the ridges in the image. While SP5 and PRM4 showed completely intercalated system. Nanoparticles showed agglomeration in some parts of the composite films due to the conformation of the polymer chains adhered to the nanoparticles.

Particle sizes on the TEM images are worth noting. In Figure 12, several ORM particles in PVA are ~8 nm , in Figure 13, BRM in PVA are as small as ~12 nm, and in Fig. 14, PRM in PVA ranges to a size of ~23 nm. Thus, it could be inferred, that there were numerous platelets that were expanded by the penetration of polymer chains.

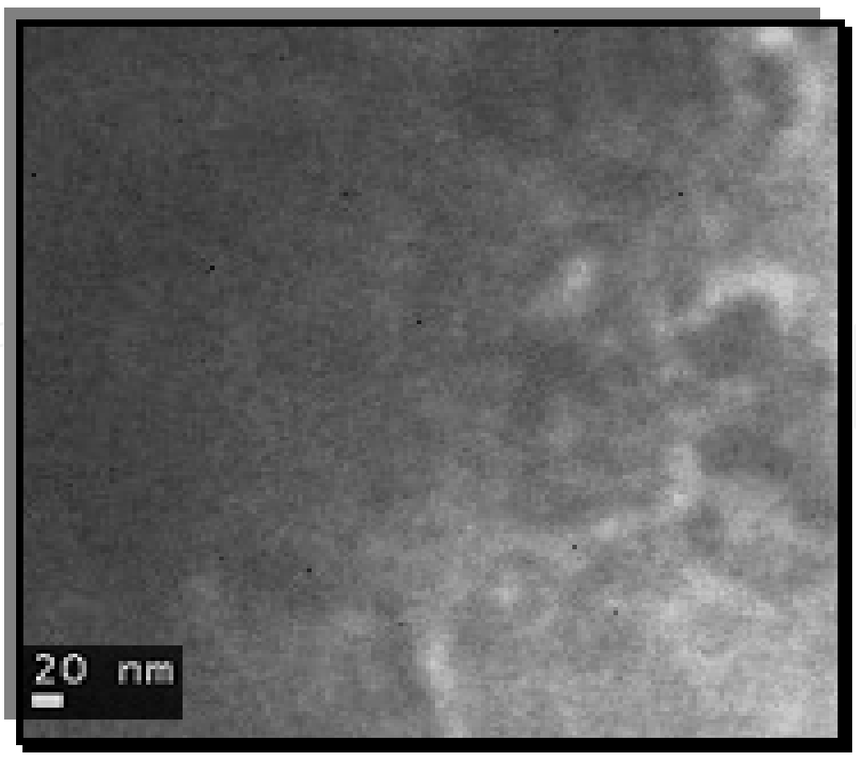

Fig. 12. TEM micrographs of CP4

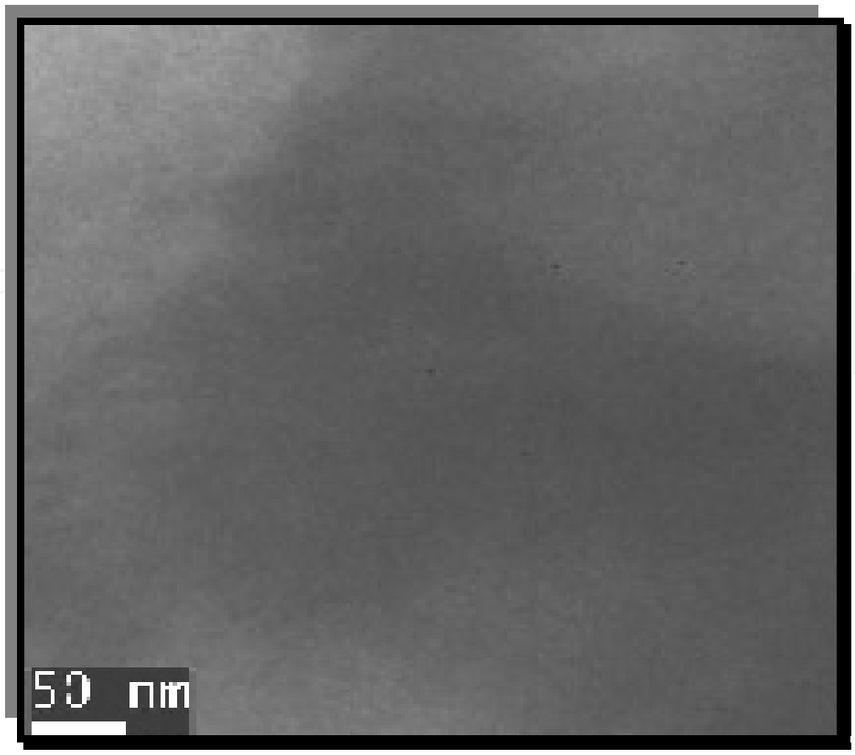

Fig. 13. TEM micrographs of SP5

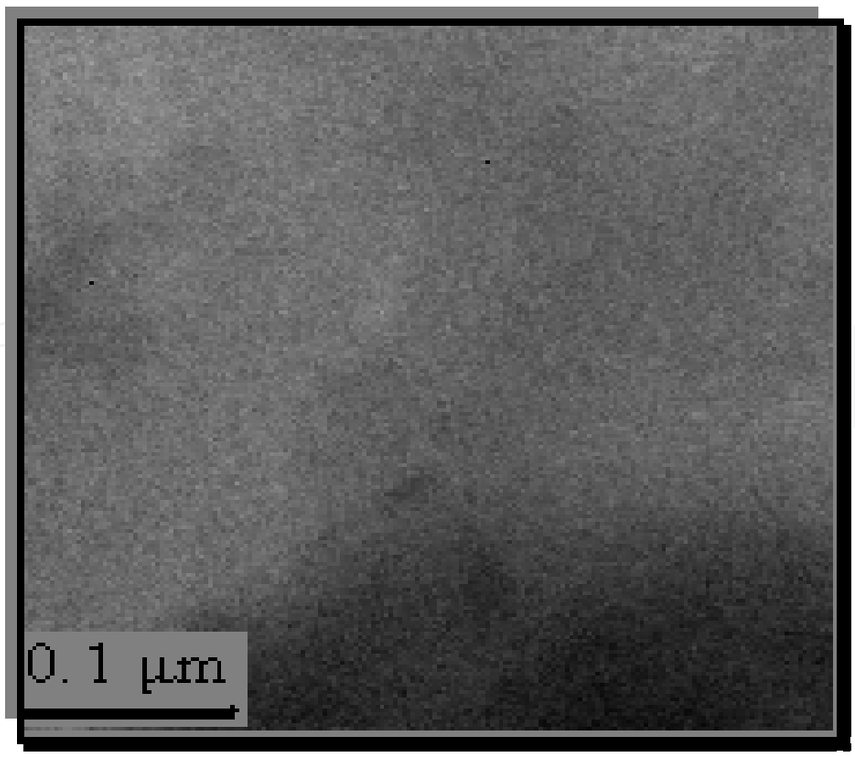

Fig. 14. TEM micrographs of PRM4

3.7 Atomic Force Microscopy (AFM)

The surface morphology of the pure PVA membrane and the PVA-modified nanocomposite membranes were analyzed by Tapping Mode - Atomic Force Microscopy (TM-AFM). Quantitatively, the differences in the morphology can be expressed in terms of various roughness parameters such as the mean roughness R_a, the root mean square (rms) of vertical data R_q, and the maximum height R_{max}. Here, the mean roughness is the mean value of surface relative to the center plane, the plane for which the volume enclosed by the image above and below this plane are equal; R_{max} the height difference between the highest and lowest points on the surface relative to the mean plane and R_q is the standard deviation of the Z values within the given area. The roughness parameters were calculated for pure PVA and PVA nanocomposite membrane surfaces with critical loading of filler and have been summarized in tabular format.

The TM-AFM images of the Pure PVA membrane is depicted in Fig. 15. The AFM images of PVA membrane shows randomly distributed hard crystalline regions (crystallites) of 100 – 250 nm in dimension on the membrane surface as evident from the observed morphology. The pure PVA membrane surface has a mean roughness of 1.026 nm.

The nanocomposite membrane with critical loading percentage of 3 wt. % BRM content (Fig. 16) shows a homogeneous and non-porous morphology. The mean roughness for the surface topography of the membrane was found to be 6.595nm. This shows that there is a good compatibility between the filler (BRM) and the PVA matrix. While critical loading surface topography of CP4 and PRM4 as shown in Fig. 17 and 18 respectively again showed homogenous and non-porous morphology. The mean roughness of CP4 and PRM4 were observed to be 2.016 nm and 9.22 nm respectively as shown in table 9.

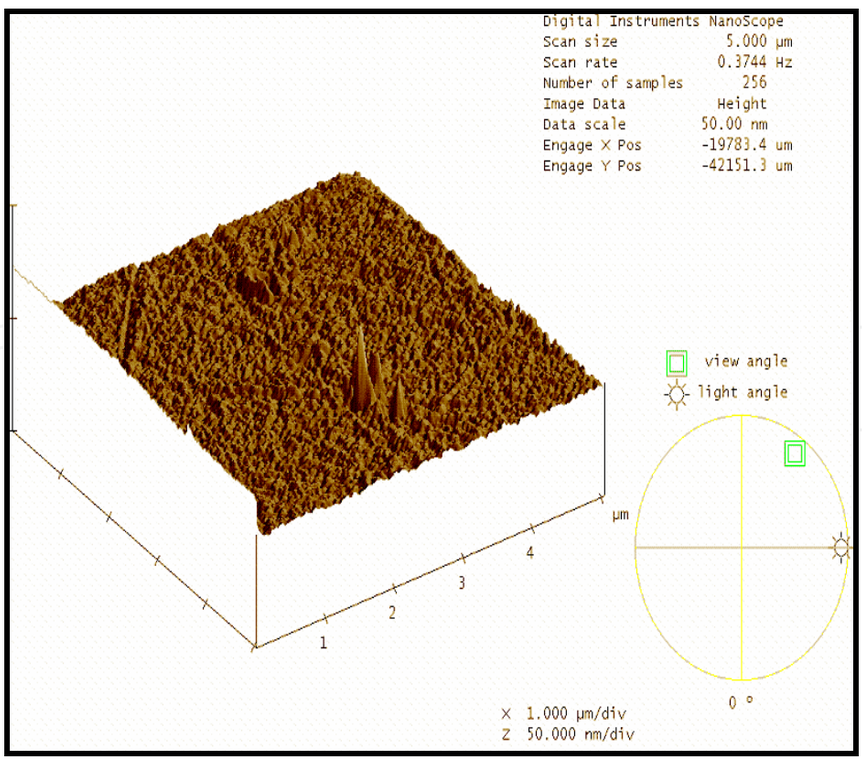

Fig. 15. Tapping Mode (3D) AFM images of Pure PVA membrane

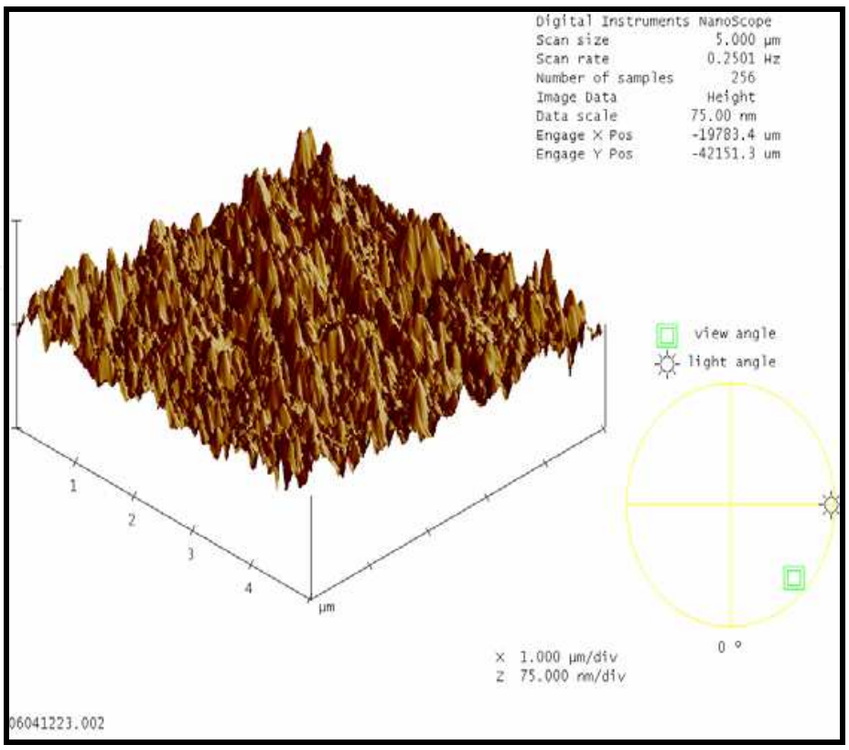

Fig. 16. Tapping Mode (3D) AFM images of SP5

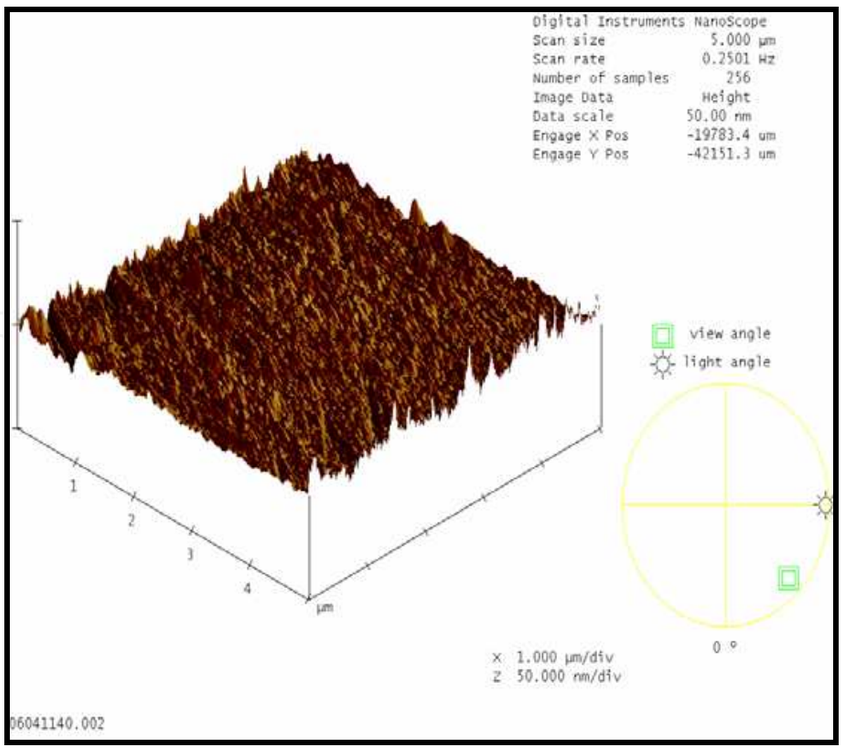

Fig. 17. Tapping Mode (3D) AFM images of CP4

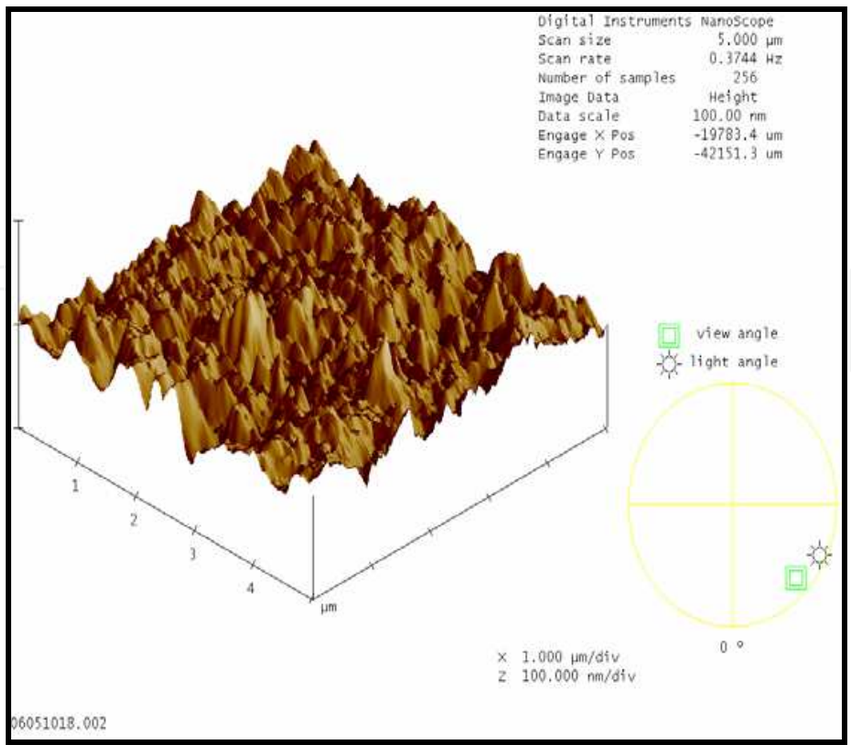

Fig. 18. Tapping Mode (3D) AFM images of PRM4

Membrane Details	R_a (nm)	R_{max} (nm)	R_q (nm)
Pure PVA	1.026	47.829	1.953
CP4	2.167	38.766	2.846
SP5	6.595	107.72	8.731
PRM4	9.22	89.803	11.572

Table 9. Roughness parameters for Pristine PVA and the PVA nanocomposite membrane surfaces

3.8 Thermogravimetric properties

The thermal stability of the raw red mud, ORM, pure PVA and PVA nanocomposite membranes with different filler content was investigated by thermogravimetric analysis. The TGA thermograms of the raw red mud, ORM, and PVA- nanocomposite films are shown in Fig. 19, Fig.20 and Fig. 21 respectively. The raw red mud is thermally stable up to 267 °C while ORM is stable upto 243 °C. Although ORM has 37% residue at 600°C, raw red mud is more stable, with 88% residue at 600°C.Raw red mud suffers an 11% weight loss at 600°C because of the probable loss of volatile impurities.

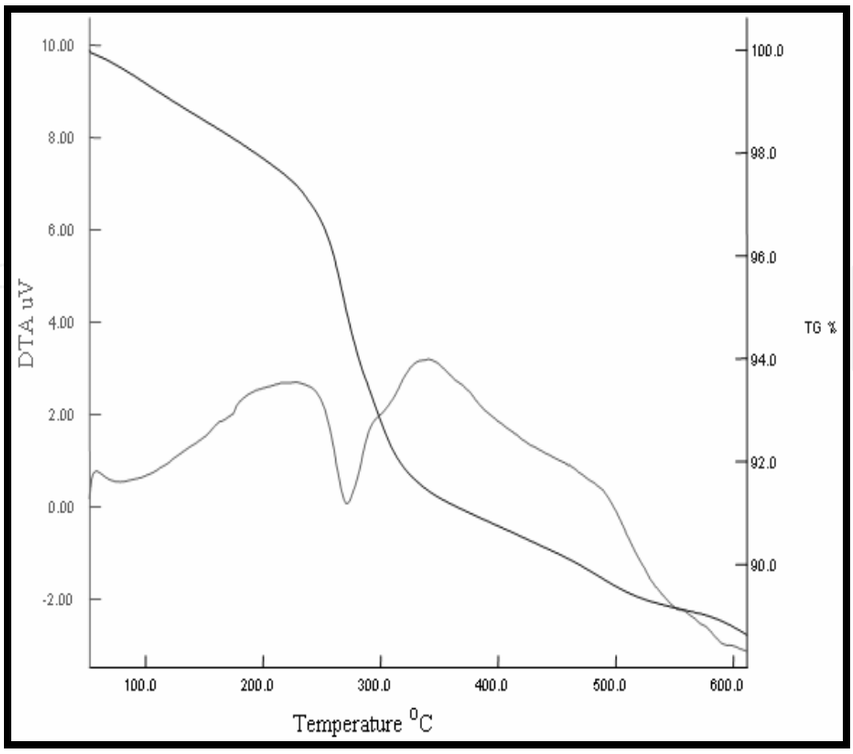

Fig. 19. DTA-TG Analysis of Raw red mud

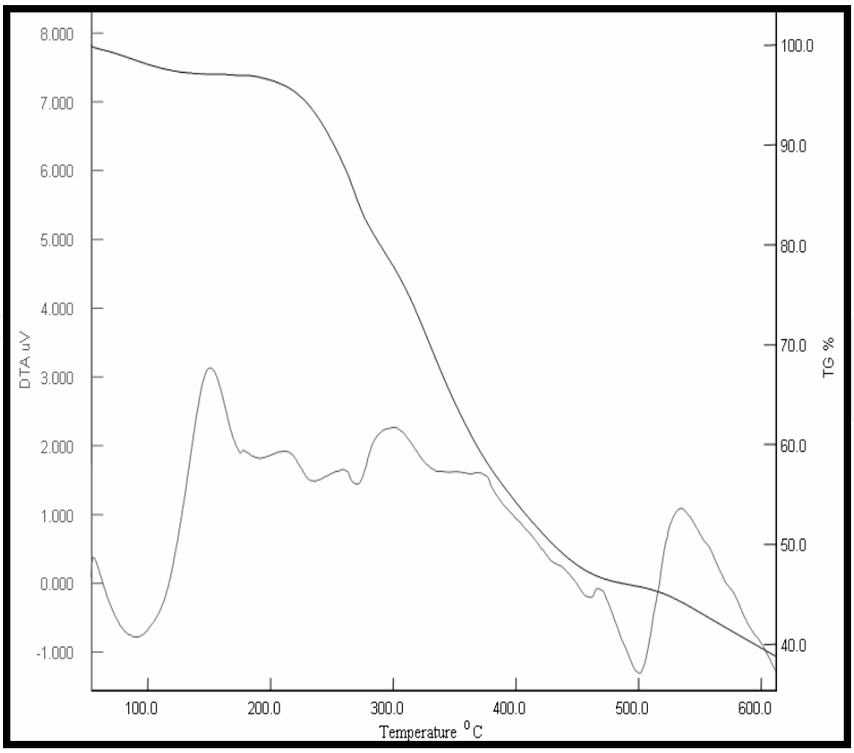

Fig. 20. DTA-TG Analysis of ORM

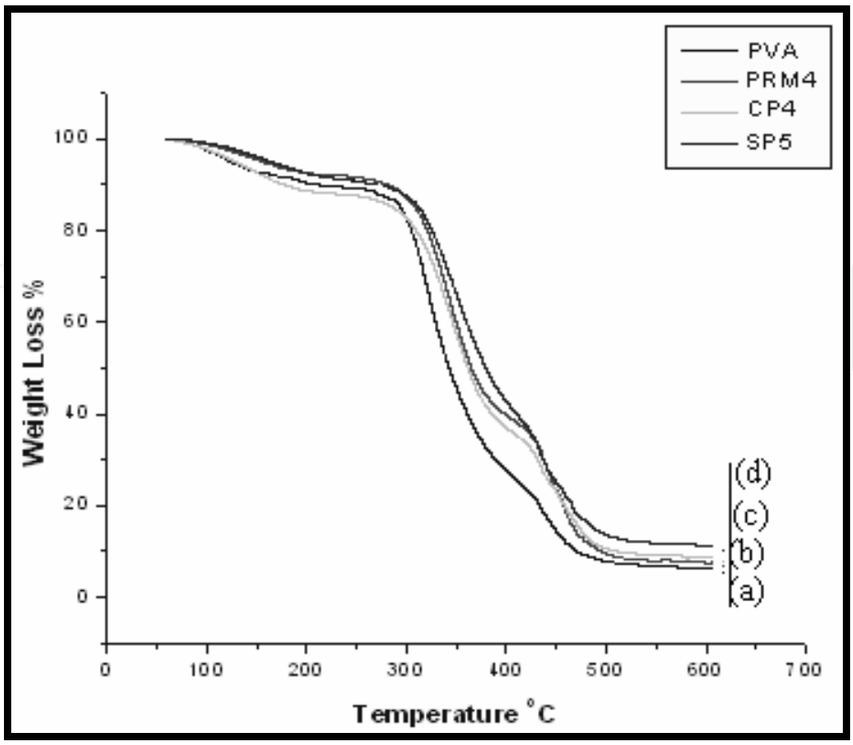

Fig. 21. Shows thermograms of (a) PVA (b) PRM4 (c) CP4 (d) SP5 film

Sample	T_i (°C)	T_f (°C)	Ash (%)
Raw red mud	267	356	88
ORM	243	482	37
Pure PVA	252	442	4.12
PRM4	274	462	7.23
CP4	277	467	10.13
SP5	281	474	12.43

Table 10. Degradation temperatures and ash content of the raw red mud, ORM, Pristine PVA and the PVA-nanocomposite membranes

The pristine PVA is thermally stable up to 250 °C. The PVA nanocomposite membranes show enhanced thermal stability; the thermal degradation of the PVA nanocomposites generally showed two major weight loss steps. The first weight loss of 15-20 wt % is centered on 150 °C and corresponds to weight loss of absorbed water and structural water of the polymer nanocomposite membranes. The weight losses in the temperature ranges of 353–483°C can be attributed mainly to the subsequent structural decomposition of the polymer backbones at higher temperatures. Evidently, the thermal decomposition of the polymer nanocomposite materials shift slightly towards the higher temperature range than that of pure PVA, which confirms the enhancement of thermal stability of intercalated polymer [Lee & Jang, 1996]. The Polymer nanocomposite membrane with critical loading of SP5, showed better thermal stability as compared to CP4 and PRM4. This could be due to better intercalation of polymer matrix within the silicate galleries of SP5 while in case of

CP4, inspite of partial exfoliation and intercalation, thermal stability is considerably lesser than SP5 .This could be due to presence of organic moiety in CP4 which causes a decrease in its thermal stability. After, 500^{o}C, the curve all became flat and mainly the inorganic residue (i.e. Al2O3, MgO, and SiO2) remained.

3.9 Differential scanning calorimetry

DSC traces of PVA and polymer nanocomposite materials are shown in Fig.22. PVA exhibited an endotherm at 52.^{o}C corresponding to the glass transition temperature (T_g) of PVA [90]. All the nanocomposite materials with different critical loading percentage of modified red mud were found to have a high T_g compared to the bulk PVA. This could tentatively be attributed to the confinement of the intercalated polymer chains within the red mud galleries that prevents the segmental motions of the polymer chains, thereby enhancing the glass transition temperature of the polymer matrix. The nanocomposite membrane SP5 showed maximum T_g and melting temperature (T_m) of 68 ^{o}C and 207 ^{o}C respectively. Thereby, revealing efficient dispersion of BRM within the polymer matrix.. The glass transition temperature (T_g) and melting temperature (T_m) of pure PVA and PVA nanocomposite membranes have been tabulated in table 11.

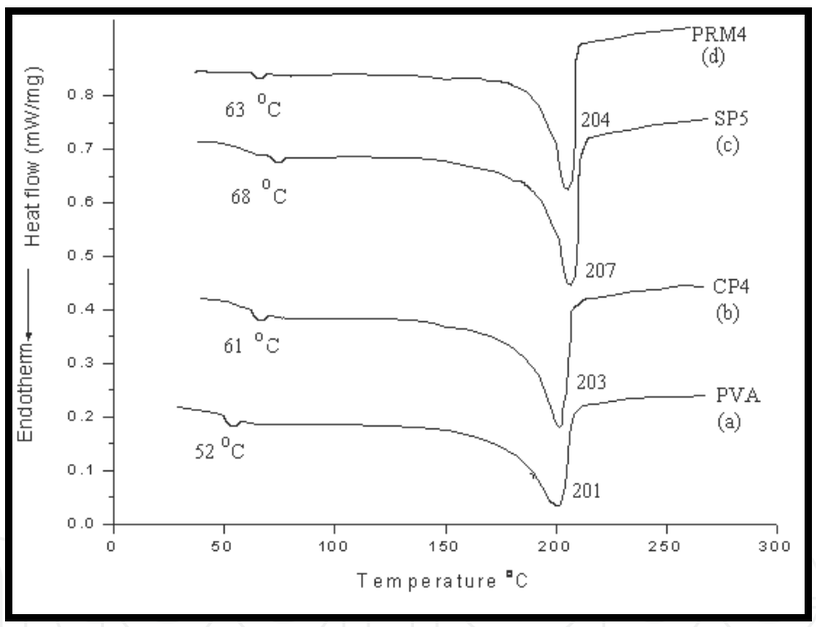

Fig. 22. DSC thermograms of (a) PVA (b) CP4 (c) SP5 (d) PRM4

Sample	T_g (^{o}C)	T_m (^{o}C)
Pure PVA	52	201
CP4	61	203
SP5	68	207
PRM4	63	204

Table 11. Glass Transition temperature (T_g) and melting temperature of pure PVA and the PVA- nanocomposite membranes

4. Preparation of Phe-phosphomolybdic acid modified red mud nanocomposite materials (PRC) and Phe-organically modified red mud nanocomposite materials (PNC)

10% (w/v) solution of Phe was prepared by dissolving dried Phe in THF with continuous stirring at 50 ^{o}C. Polymer nanocomposite (PN) films were made by mixing different loading percentage of phosphomolybdic acid modified red mud (PRM) and organically modified red mud (ORM) into the virgin Phe solution, stirred constantly and sonicated for half an hour for better dispersion. The composition of the PN materials was varied from 0 to 3wt % of modified RM with respect to the Phe content. The samples were designated as shown in Table 12.

Sample index	% Loading of filler
*Phe	0
**PRC1	1.0
PRC2	2.0
PRC3	3.0
***PNC1	1.0
PNC2	2.0
PNC3	3.0

*Phe: Phenoxy or poly (hydroxy ether) of Bisphenol A
** PRC: Phe-phosphomolybdic acid modified red mud nanocomposites
*** PNC: Phe-organically modified red mud nanocomposites

Table 12. Sample Designation

4.1 FTIR spectroscopy

The FTIR spectra in Figure 23 showed the presence of characteristic peaks of poly (hydroxy ether) of bisphenol A. The characteristic vibration band of Phe for hydroxyl stretching vibration (O-H) having polymeric association was observed at 3394 cm^{-1}, While the alkyl stretching band of C-H was shown at 2974 cm^{-1} and aryl stretching band of C-H at 3037 cm^{-1}. The peak at v = 1183 cm^{-1} is due to C-O stretching of phenyl ether linkage. Further, the peak at v = 1607 cm^{-1} could be attributed to the aromatic ring.

Figure 23 also showed the spectra of Phe-modified red mud nanocomposite membranes with different loading percentage of the filler. The characteristic vibration band of PRC3 for hydroxyl stretching vibration (O-H) was observed at 3270 cm^{-1}. The intensity of the O-H stretching vibration peak decreased and peak frequency shifted from 3394 to 3270 cm^{-1}, i.e. to a lower frequency as compared to that of pure phenoxy. The red shift in the hydroxyl stretching frequency occurs due to the various degree of hydrogen bonding between the polymer and the filler which lengthens and weakens the O-H bond and hence lowers the vibrational frequency. The alkyl stretching band of C-H in case of PRC3 also showed red shift from 2974 to 2861 cm^{-1} due to the interaction of modified red mud with the polymer matrix. Similarly, peak at v = 3036 cm^{-1}, was attributed to the stretching vibration of aryl C-H band, slightly lower frequency than the pure phenoxy. The other characteristic vibrational frequencies of PRC3 are presented in table 13.

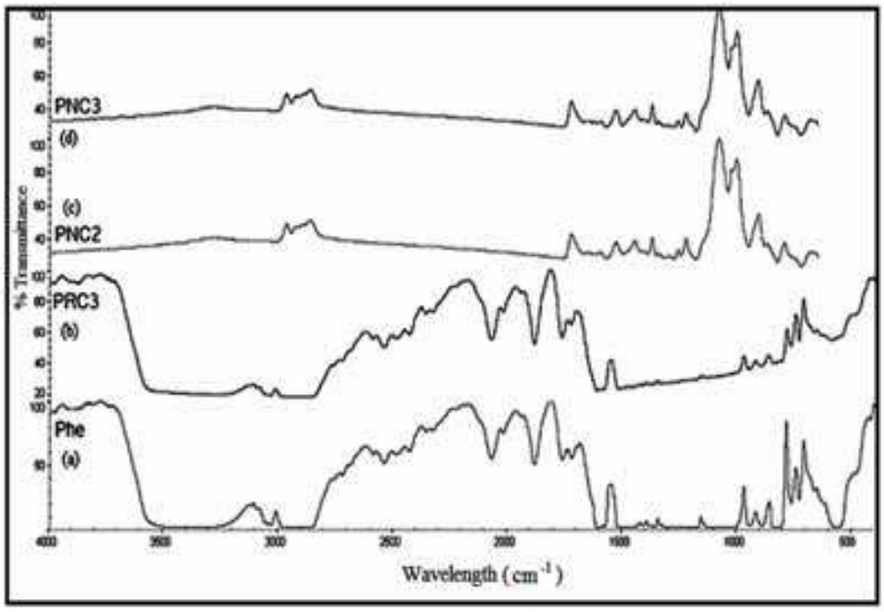

Fig. 23. FTIR Spectrum of (a) Pure Phe (b) PRC3 (c) PNC2 (d) PNC3

Groups	PHE (cm^{-1})	PRC3 (cm^{-1})	PNC2 (cm^{-1})	PNC3 (cm^{-1})
OH	3394	3270	-	-
C-H	2974	2861	2948	2947
C-H (Ar)	3037	3036	3016	3020
NH_3+	-	-	1571	1572
C-O	1183	1168	1182	1180
C=O	-	1766	1760	1760
Ar	1607	1613	1499	1503
Si-O	-	953	952	951
Mo-O_c-Mo	-	896	-	-

Table 13. Assignment of FTIR spectral bands for Pure Phenoxy and the Ph/modified red mud nanocomposite membranes

The spectra of PNC2 and PNC3 as shown in fig. 23, showed the disappearance of the hydroxyl stretching frequency (O-H). The disappearance of the hydroxyl peak depicted complete physical interaction of the O-H group with different groups of the organically modified red mud, thereby not leaving any free hydroxyl group. However, alkyl stretching band of C-H for PNC2 and PNC3 were observed at 2948 and 2947 cm^{-1} respectively. The red shift in the alkyl stretching frequency C-H of PNC2 and PNC3 as compared to the pure phenoxy showed interaction of the filler with the polymer matrix.

The characteristic vibrational frequencies of PNC2 and PNC3 at ν = 1571 and 1572 cm^{-1} respectively, was attributed to the stretching frequency of ammonium ion (NH_3^+), thereby

depicting formation of zwitter ion. The other vibrational frequencies associated with PNC2 and PNC3 have been tabulated in table 13. The organically modified red mud(ORM) showed better interaction with the poly (hydroxy ether) of bisphenol A matrix as compared to phosphomolybdic acid modified red mud (PRM), therefore, it can be inferred that ORM will show better dispersion into the polymer matrix as compared to PRM.

4.2 X - ray diffraction study

The wide angle diffraction pattern of PRC2 and PRC3 films are shown in Fig. 5. The crystallinity of the composite membranes is mainly due to Phe. The characteristic diffraction peak for PRC2 and PRC3 were observed at a 2θ value of 2.36° and 2.26°. The diffraction peak at 2θ = 2.26 ° is considerably broadened and the interplanner distance has also widened compared to the raw red mud and PRC2 nanocomposite, indicating intercalation of the phenoxy matrix within the nanofiller of the nanocomposite membranes.

The polymer nanocomposite films showed decrease in the intensity of the crystalline peak as the loading percentage of organically modified red mud increased. The decrease in the intensity of crystalline peaks showed an increase in the disorderness of the interlayers of modified red mud.

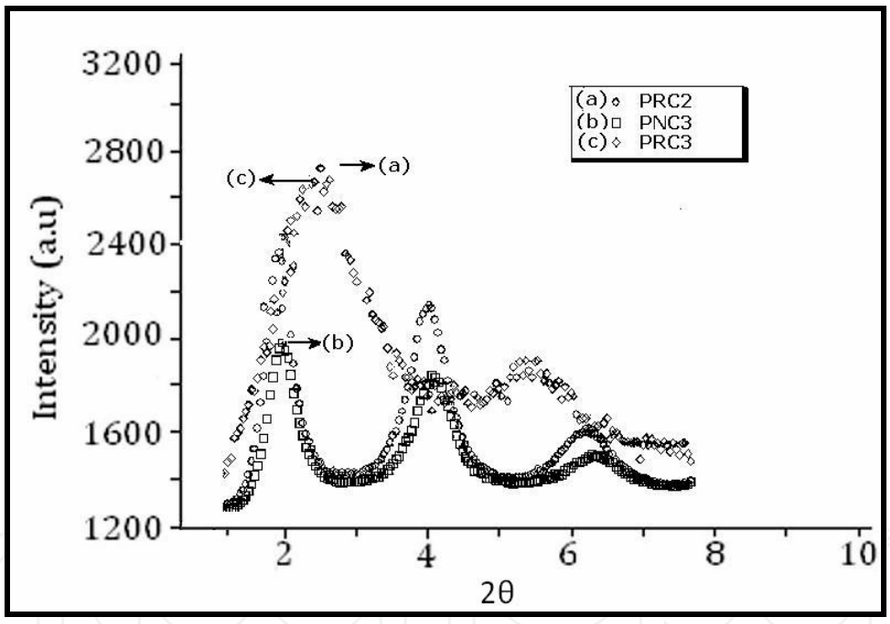

Fig. 24. XRD pattern of (a) PRC2 (b) PNC3 (c) PRC3 nanocomposites

From table 14, it is clear that the basal spacing for PRC3 is larger than the other PRM based nanocomposites materials, thereby giving evidence of better intercalation of polymer matrix within the silicate galleries of filler in case of PRC3 than the rest of nanocomposites.

Sample	2θ	d-spacing (A°)
PRC2	2.36	37.56
PRC3	2.26	39.48
PNC3	2.11	41.62

Table 14. XRD results of Phe-PRM and Phe-ORM based nanocomposite membranes

The X-ray diffraction pattern of phenoxy-organically modified red mud nanocomposite membranes are shown in fig. 24.The characteristic diffraction band of PNC3 was observed at $2\theta = 2.11^{o}$. The increase in the interlayer distance of silicate galleries of the organically modified red mud indicated that Phe has successfully intercalated into the silicate layers.

4.3 Field Emission Scanning electron microscopy (FESEM)

Field emission scanning electron microscope has evolved in which the electron beam cross section has become smaller and smaller increasing magnification several fold. Raw red mud and modified red mud were characterized by Field Emission Scanning Electron Microscopy (FESEM), as shown in Figure25. The FESEM analysis showed that the raw red mud consisted of aggregates, including particles of different dimensions. The FESEM image of the PRM and ORM showed a very fine distribution of particles with a size of 64 and 71 nm respectively as shown in Fig. 7. While ORM showed a homogenous distribution of particles than raw red mud with particle size larger than PRM due to formation of organic coating around the particles.

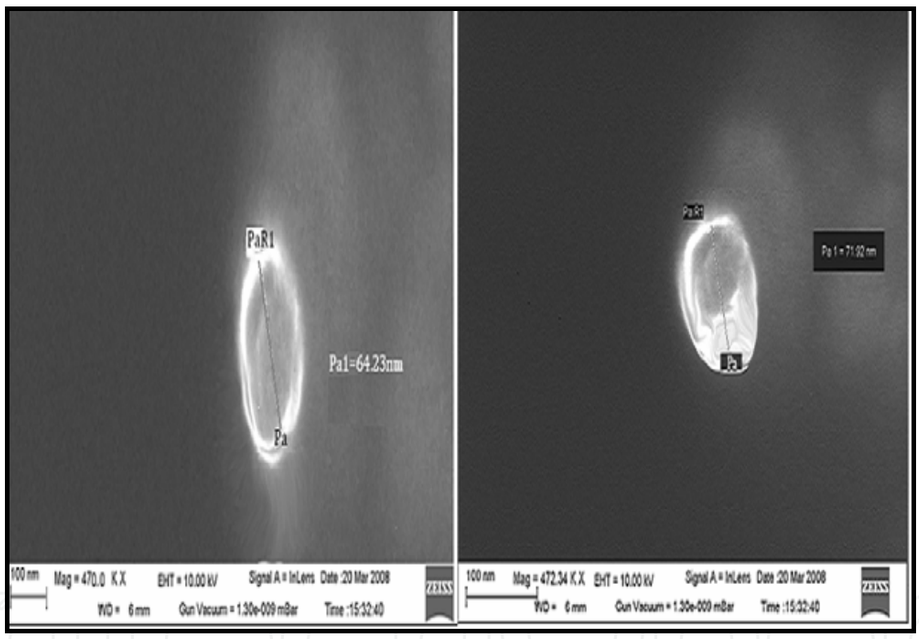

Fig. 25. FESEM images depicting size of a single red mud particle (a) Phosphomolybdic acid modified red mud (PRM), (b) Organically modified red mud (ORM)

4.4 Transmission Electron Microscopy (TEM)

TEM complements XRD by observing a very small section of the material for the possibility of intercalation or exfoliation. It also provides information about the particle size and nanodispersion of particles. It however, supplies information on a very local scale. However, it is a valuable tool because it enables us to see the polymer and the filler on a nanometer scale.

Fig. 8 (a) showed a representative TEM image of the PNC3 with a 3 wt% loading percentage of organically modified red mud in the phenoxy matrix, while fig. 8(b) showed a representative TEM image of PRC3. As seen in fig. 8(a), a rather good dispersion of the

organically modified red mud is achieved. It is clear that the area covered by the red mud in fig.8 (a) is larger than in fig. 8(b) indicating a more extended platelet separation and an overall best nanodispersion of the critical loading of 3 wt% ORM in the phenoxy matrix.

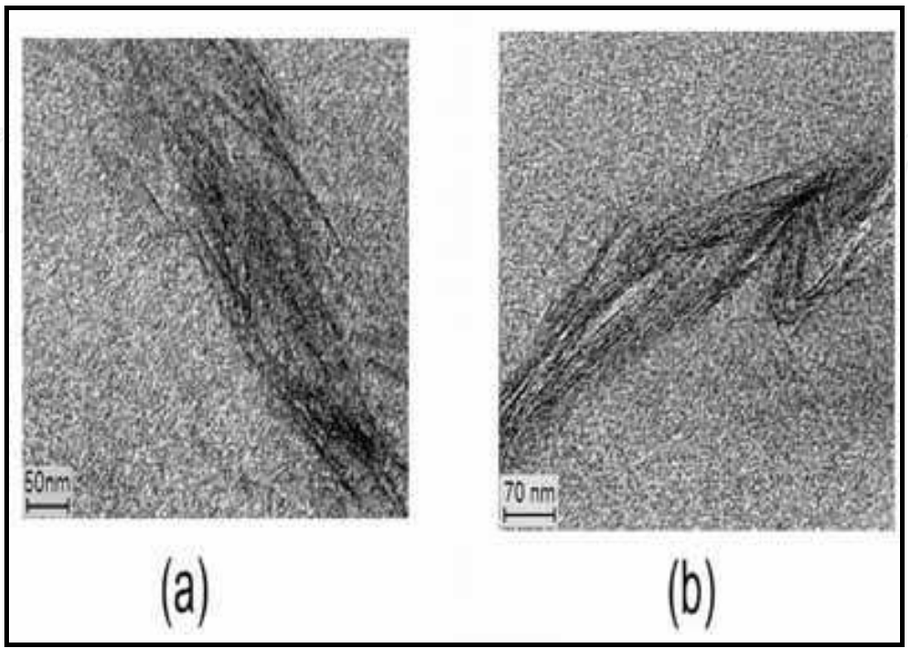

Fig. 26. TEM micrographs of (a) PNC3 (b) PRC3

The average particle size was found as 14 nm in case of PNC3 as shown in fig. 26(a), while the size of the particles in PRC3 was found to be 19 nm as shown in fig. 26(b). In fig. 26(b), the nanoparticles showed certain extent of agglomeration and formation of interconnected aggregates or tactoids of silicates.

There may be several fundamental problems that affect the polymer particle interactions in solution, resulting in disordered nanoparticle aggregates. These problems may arise from competing interactions between solvent, polymer chains and filler particles. The conformation of the polymer chains adhered to the nanoparticles also influences the ordered dispersion of the particles.

The presence of the organically modified red mud and phosphomolybdic acid modified red mud with different loading percentage and dispersing capabilities, may help us to identify the main structural driving force for dispersion in these Phe based PNs. It has been reported that the interaction between the polymer chains and the inorganic surface of the clay (Fornes et al., 2004) is crucial in polar polymers, and therefore it could also exist between the polar Phe and the modified red mud surface. Good dispersion of modified red mud in the polymer matrix will have a significant effect on the properties of the nanocomposites.

4.5 Thermogravimetric properties

The thermal stability of the pure Phe and Phe nanocomposite membranes with different filler content was investigated by thermogravimetric analysis. The TGA thermograms corresponding to the thermal decomposition of pure Phenoxy and Phe- nanocomposite films are shown in fig. 27 and fig. 28.

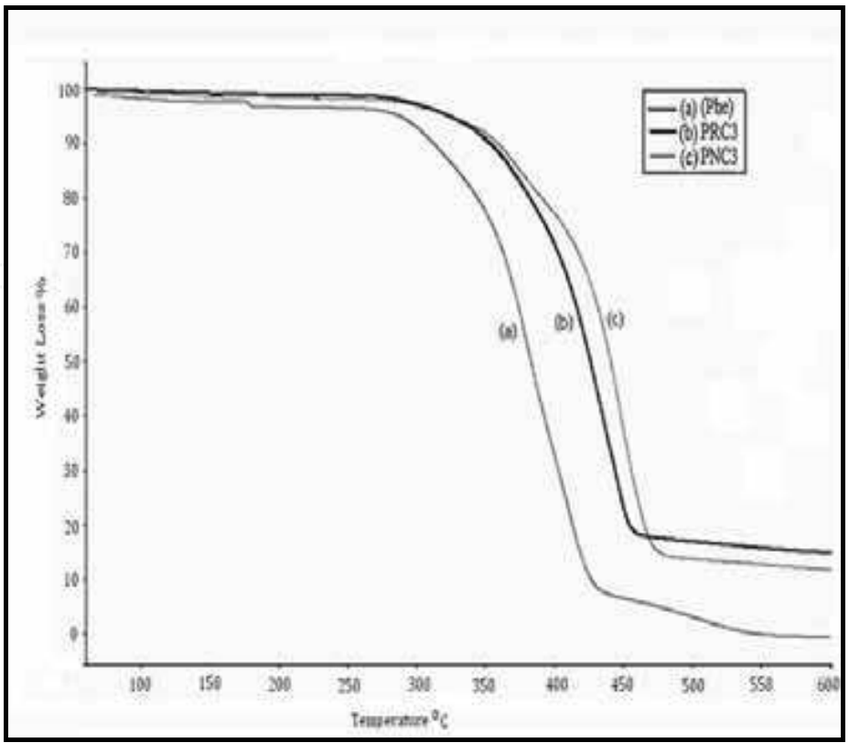

Fig. 27. Thermograms of (a) Phe (b) PRC3 (c) PNC3

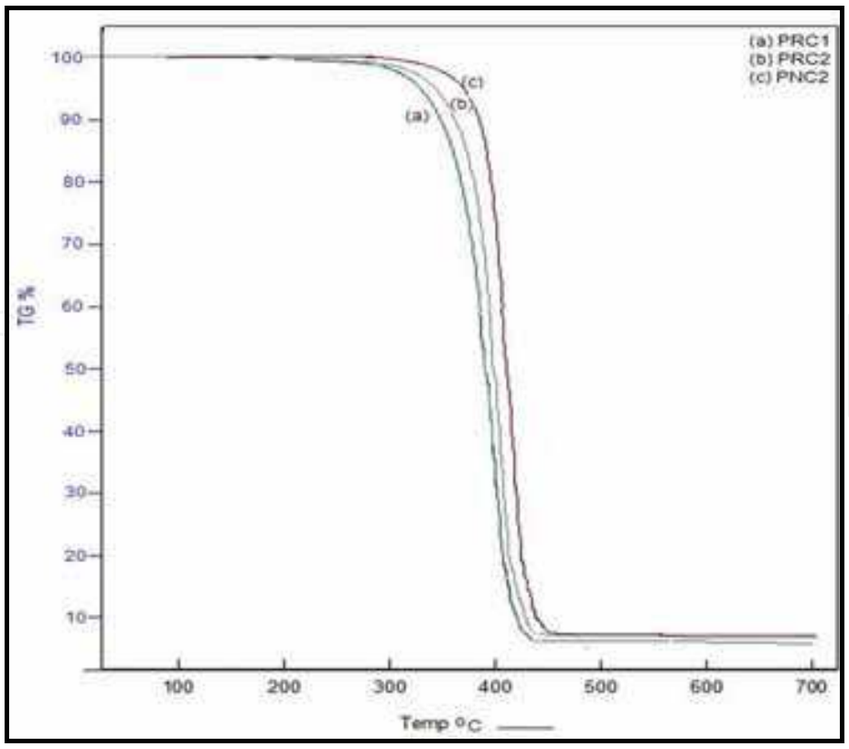

Fig. 28. Shows typical THA thermograms of (a) PRC1 (b) PRC2 (c) PNC2

As can be observed, both pure polymer and nanocomposite materials decompose in a single stage. If we compare the thermal stability of the polymer and the critical loading percentage nanocomposite membranes of PNC3 and PRC3, it is clear that PNC3 is more stable than pure Phenoxy and PRC3. The pristine Phe is thermally stable up to 275 ^{o}C. Since, the Phe nanocomposite membranes show enhanced thermal stability, the initial decomposition temperature (T_i) of phenoxy occurred at 276 ^{o}C while in case of PNC3 and PRC3, T_i was found at 318 and 298 ^{o}C respectively as shown in table 15. Similarly, final decomposition temperature (T_f) of phenoxy, PNC3 and PRC3 were observed at 433, 479 and 458 ^{o}C respectively. The enhancement in the thermal stability of PNC3 could be attributed to the better compatibility and intercalation of polymer matrix within the silicate galleries of 3 wt% organically modified red mud. Similarly, from fig.28 and table 15, it was observed that PNC2 showed higher Ti and Tf as compared to the PRC1 and PRC2, thereby showing higher thermal stability comparatively.

In general, major weight losses were observed in the range of 275–500 oC for Phe and polymer nanocomposite films, which may be correspondent to the structural decomposition of the polymer backbones at higher temperatures. After 500oC, all the curves became flat and mainly the inorganic residue (i.e. Al2O3, MgO, and SiO2 etc.) remained.

Sample	T_i (^{o}C)	T_f (^{o}C)	Ash (%)
Pure Phe	276	433	3.2
PRC1	287	439	6.33
PRC2	293	443	7.97
PNC2	312	454	8.23
PNC3	318	479	11.30
PRC3	298	458	14.15

Table 15. Degradation temperature and ash content of Pristine Phe and the Phe-nanocomposite membranes

4.6 Atomic Force Microscopy (AFM)

The surface morphology of the pure Phenoxy membrane and the Ph-modified nanocomposite membranes were analyzed by Tapping Mode - Atomic Force Microscopy (TM-AFM). Quantitatively, the differences in the morphology can be expressed in terms of various roughness parameters such as the mean roughness R_a, the root mean square (rms) of vertical data R_q, and the maximum height R_{max}. Here, the mean roughness is the mean value of surface relative to the center plane, the plane for which the volume enclosed by the image above and below this plane are equal; R_{max} the height difference between the highest and lowest points on the surface relative to the mean plane and R_q is the standard deviation of the Z values within the given area. The roughness parameters were calculated for pure Ph and Ph nanocomposite membrane surfaces with critical loading of filler and have been summarized in tabular format.

The TM-AFM images of the Pure Phe membrane is depicted in Fig. 29. The AFM images of Phe membrane showed randomly distributed hard crystalline regions (crystallites) of 50 – 200 nm in dimension on the membrane surface as evident from the observed morphology. The pure Phe membrane surface has a mean roughness of 3.297 nm.

The nanocomposite membrane with critical loading percentage of 3 wt. % ORM (i.e., PNC3) content (Fig. 29) showed a homogeneous and non-porous morphology. The mean roughness for the surface topography of the membrane was found to be 4.045 nm.

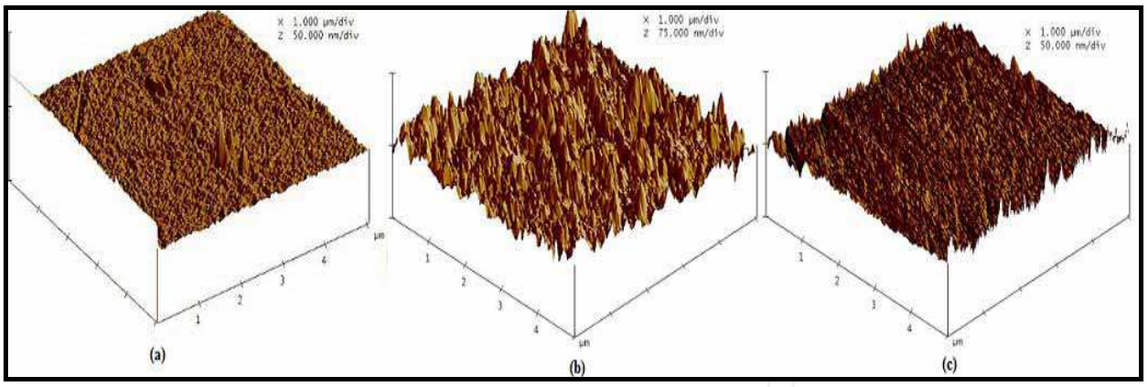

Fig. 29. Tapping mode (3D) AFM images of (a) Phe (b) PRC3 (c) PRC2

This shows that there is a good compatibility between the filler (ORM) and the Ph matrix. This is in consistent with the results of SEM studies. While critical loading surface topography of PRC3 showed some non-uniform regions with non-porous morphology. The mean roughness of PRC3 was observed to be 4.562 nm as shown in table 16. This showed that the phosphomolybdic acid modified red mud with 3 wt% loading percentage tends to form some aggregated particles within the polymer matrix leading to higher roughness values as compared to the PNC3.

Sample	R_a (nm)	R_{max} (nm)	R_q (nm)
Pure Ph	3.297	27.668	4.173
PNC3	4.045	57.648	5.497
PRC3	4.562	116.65	7.003

Table 16. Roughness parameters for Pristine Ph and the Ph nanocomposite membrane surfaces

4.7 Differential Scanning Calorimetry (DSC)

DSC traces of pure Phenoxy and polymer nanocomposite materials are shown in Fig.30. Ph exhibited a shallow endotherm at 61°C corresponding to the glass transition temperature (T_g) of Ph. All the nanocomposite materials with different critical loading percentage of modified red mud were found to have a high T_g as compared to the pristine Phe. This could be attributed to the confinement of the intercalated polymer chains within the red mud galleries that prevents the segmental motions of the polymer chains, thereby enhancing the glass transition temperature of the polymer matrix. The PNC3 nanocomposite membrane showed maximum T_g and melting temperature (T_m) of 66 °C and 220 °C respectively. This depicted that PNC3 is thermally more stable than PRC3 nanocomposite membrane on account of better dispersion and adhesion of the ORM within the polymer matrix. The glass transition temperature (T_g) and melting temperature (T_m) of pure phenoxy and Ph nanocomposite membranes have been tabulated in table 17.

Sample	T_g (°C)	T_m (°C)
Pure Phe	61	206
PNC3	64	211
PRC3	66	220

Table 17. Glass Transition temperature (T_g) and melting temperature of pure Phe and Phe-nanocomposite membranes

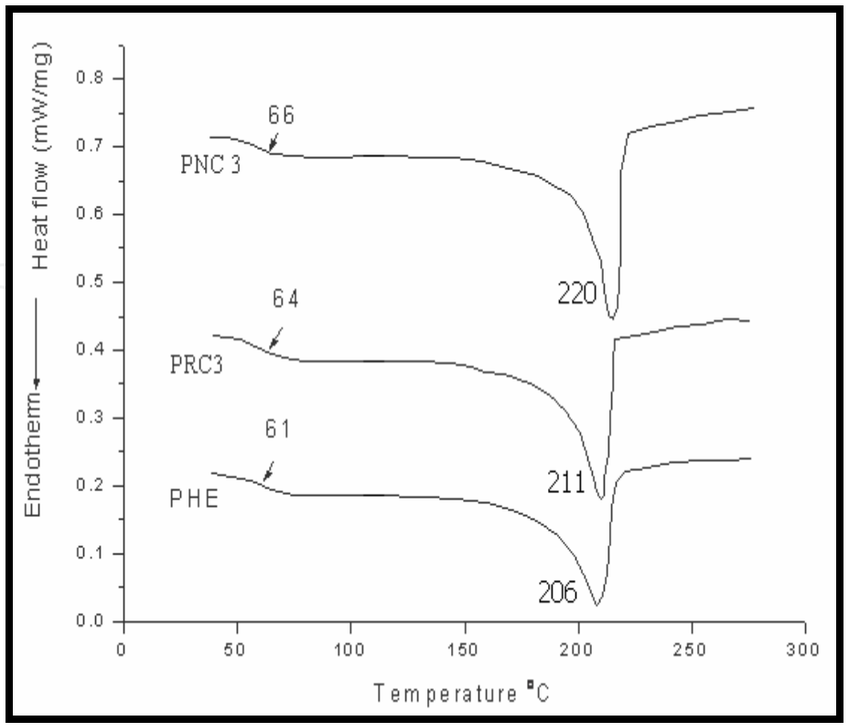

Fig. 30. DSC thermograms of (a) Ph (b) PRC3 (c) PNC3

4.8 Conclusion

- Red mud was successfully modified with the inorganic acids and organic moiety (aniline formaldehyde). The modification ameliorates both the dispersion level and the material properties of the polymer nanocomposites.
- The PVA- boric acid modified red mud nanocomposite films showed better glass transition temperature T_g and thermal stability at a filler concentration of 3.0wt percentage.
- In PVA/ORM nanocomposite systems, 2.0wt% modified red mud (CP4) based nanocomposite film exhibited relatively good dispersion with increase in the thermal stability, glass transition temperature.
- In PVA/PRM nanocomposite systems, 2.5wt% modified red mud (PRM4) based nanocomposite film exhibited relatively good dispersion with increase in the material properties as compared to the pristine poly (vinyl alcohol).
- PVA based nanocomposites showed an increase in the roughness values with the increase in the filler content but the 3.0wt% of boric acid modified red mud nanocomposite membrane showed lower roughness values as compared to the critical loading percentage of ORM and PRM based nanocomposites.
- On comparing the material properties of all the three nanocomposite systems, it was found that the critical loading percentage of BRM based nanocomposite system (i.e., SP5) showed better enhancement as compared to the critical loading percentage of ORM and PRM based nanocomposite systems.
- The TEM images of the PVA-modified red mud nanocomposite membranes showed homogeneous nano phase dispersion of the modified red mud in the PVA polymer matrices at a scale of 8- 23 nm particle size.

- In the poly(hydroxy ether of bisphenol A) (Phe) based nanocomposites as reported in this work, mostly intercalated structures were produced in the acid modified red mud modifications, but modification by organic moiety (ORM) resulted in a mixed intercalated-exfoliated structure.
- Thermal stability of polymer also increases after nanocomposites preparation, because red mud acts as a heat barrier, which enhances the overall thermal stability of the system, as well as assist in the formation of char after thermal decomposition.
- Phe based nanocomposites showed an increase in the roughness values with the increase in the filler content but the 3.0wt% of organically modified red mud nanocomposite membrane showed lower roughness values as compared to the critical loading percentage of PRM based nanocomposites. Thus, PNC3 showed homogenous and non-porous morphology as compared to the coarse morphology of PRC3 type of nanocomposites.
- The average particle size in case of PNC3 is 14 nm while the particle size of PRC3 is 19 nm as revealed by TEM studies.

5. References

Agag, T.; Koga, T.; Takeichi, T. (2001). Studies on thermal and mechanical properties of polyimide–clay nanocomposites, *Polymer*, 42, 3399.

Alexandre, M.; Dubois P. (2000). Polymer-layered silicate nanocomposites: preparation, properties and uses of a new class of materials. *Materials Science & Engineering, R: Reports*, R28 (1-2), 1-63.

Bachtsi, A.R; Kiparissides, C. (1996). Synthesis and release studies of oil containing poly (vinyl alcohol) microcapsules prepared by coacervation, *Journal of Controlled Release*, 38 (1), 49-58.

Bhat, A.H, Banthia, A.K, (2007). Preparation and Characterization of Poly (vinyl alcohol)–Modified red mud composite materials, *Journal of Applied Polymer Science*, 103 (1), pp. 238-243.

Biron, M., (2007). Thermoplastics and Thermoplastic Composites. Elsevier Ltd., Jordan Hill, Oxford.

Chand, N.; Hashmi, S. A. R. (1999). Effect of Red Mud Addition on Abrasive Wear Rate of Isotactic Polypropylene/Low Density Polyethylene Blend under Low Stress Conditions, *JSci Ind Res*, 58, 795.

Chand, N.; Hashmi, S. A. R. (1999). Effect of addition of polycarbonate on sheared flow of red mud-filled isotactic polypropylene *Bull Mater Sci*, 22, 801.

Chen, H.L. Wu, L.G; Tan, J; Zhu, C.L.; (2000). PVA membrane filled β-cyclodextrin for separation of isomeric xylenes by pervaporation. *Chemical Engineering Journal*, 78 (2-3), 159-164.

Dilsiz, N.; Ebert, E.; Weisweiler, W.; Akovali, G. (1995). Effect of plasma Polymerization on Carbon Fibers Used forFiber/Epoxy Composites *JColloid Interface Sci*, 170, 241.

Donnet, J. B.; Bansal, R. C. Carbon Fibers, 2nd ed.; Dekker: New York, 1990.

Fornes TD, Hunter DL, Paul DR. (2004) Nylon - 6 nanocomposites from alkylammonium - modified clay: the role of alkyl tails on exfoliation. *Macromolecules*, 37(5), pp. 1793-1798.

Grjotheim, K.; Welch, B. J. Aluminium Smelter Technology: A Pure and Applied Approach, 2nd ed.; Verlag: Dusseldorf, 1998.

Hajji, P.; David, L.; Gerard, J. F; Pascault, J. P; Vigier, G. (1999). Synthesis, structure, and morphology of polymer-silica hybrid nanocomposites based on hydroxyethyl methacrylate, *Journal of Polymer Science*, Part B: Polymer Physics, 37(22), 3172-3187.

Horii,F; Hu,S; Ito,T; Odani,H; Kitamaru.R, (1992).Cross-polarization/magic-angle-spinning carbon-13 NMR study of solid structure and hydrogen bonding of poly(vinyl alcohol) films with different tacticities, *Polymer*, , 33(11), 2299-2306.

Huang, H H.; Orler, B.; Wilkes, G L. (1987). Structure-property behavior of new hybrid materials incorporating oligomeric species into sol-gel glasses. 3. Effect of acid content,tetraethoxysilane content, and molecular weight of poly (dimethylsiloxane), *Macromolecules*, 20, 1322.

Ishikawa, Y.; Matsumoto, Y. (2001). Electrodeposition of TiO2 photocatalyst into nano - pores of hard alumite *Electrochem Acta*, 46, 2819.

Jang, B. Z. (1992). Control of interfacial adhesion in continuous carbon and kevlar fiber reinforced polymer composites, *Compos Sci Technol*, 44, 333.

Kasliwal, P.; Sai, P. S. T. (1999). Enrichment of titanium dioxide in red mud: a kinetic study *Hydrometallurgy*, 53, 73.

Lee, D. C.; Jang, L. W. (1996). Preparation and characterization of PMMA-clay hybrid composite by emulsion polymerization. *Journal of Applied Polymer Science*, 61(7), pp. 1117-1122.

Novak, B. M; Ellsworth, M. W. (1993). "Inverse" organic-inorganic composite materials: high glass content non- shrinking sol-gel composites, *Materials Science & Engineering*, A: Structural Materials: Properties, Microstructure and Processing, A162(1-2), 257- 64.

Park, S. J.; Cho, M. S. (2000). Effect of anti-oxidative filler on the interfacial mechanical properties of carbon–carbon composites measured at high temperature. *Carbon*, 38, 1053.

Park, S. J.; Kim, M. H. (2000). Effect of acidic anode treatment on carbon fibers for increasing fiber - matrix adhesion and its relationship to interlaminar shear strength of composites *JMater Sci*, 35, 1901.

Park, S. J.; Kim, J. S. (2001).Influence of Plasma Treatment on Microstructures and Acid - Base Surface Energetics of Nanostructured Carbon Blacks: N2 Plasma Environment, *JColloid Interface Sci*, 232, 311.

Peppas, N.A; Merrill, E.W, (1977). Development of semicrystalline poly(vinyl alcohol) hydrogels for biomedical applications, *Journal of Biomedical Materials Research*, 11(3), 423-34.

Pradhan, J.; Das, S. N.; Thakur, R. S. (1999). Adsorption of Hexavalent Chromium from Aqueous Solution by Usin Activated Red Mud, *JColloid Interface Sci*, 217, 137.

Ray S. S and Bousmina M, (2005). Biodegradable polymers and their layered silicate nanocomposites: In *greening the 21st century materials world*, *Progress in Materials Science*, 50(8), 962-1079.

Shao, C.; Kim, H-Y; Gong, J.; Ding, B.; Lee, D-R.; Park, S-J. (2003). Fiber mats of poly(vinyl alcohol)/silica composite via electrospinning, *Materials Letters*, 57(9-10),1579-1584.

Surivet, F.; Lam, T. M ; Pascault, J. P; Pham, Q. T. (1992). Organic-inorganic hybrid materials. 1. Hydrolysis and condensation mechanisms involved in alkoxysilane-terminated macromonomers, *Macromolecules* , 25(17), 4309-20.

Yuan, L. T.; Shyu, S. S.; Lai, J. Y. (1991). Plasma surface treatments on carbon filbers. II. Mechanical property and interfacial shear strength *JAppl Polym Sci*, 42, 2525.

Zhang H, Ma H, Hongtu Li and Wang (2002). J, Synthesis and characterization of a polymer– metal complex from bisphenol A polyhydroxy ether with sulfur-bearing side-groups, *Polym Int*., 51, pp.1129–1134.

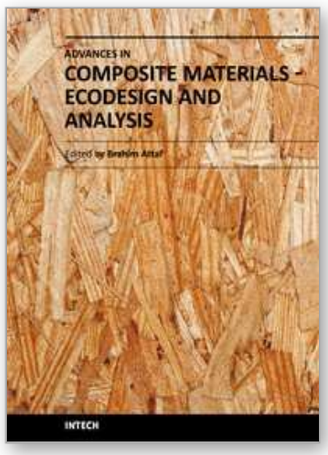

Advances in Composite Materials - Ecodesign and Analysis
Edited by Dr. Brahim Attaf

ISBN 978-953-307-150-3
Hard cover, 642 pages
Publisher InTech
Published online 16, March, 2011
Published in print edition March, 2011

By adopting the principles of sustainable design and cleaner production, this important book opens a new challenge in the world of composite materials and explores the achieved advancements of specialists in their respective areas of research and innovation. Contributions coming from both spaces of academia and industry were so diversified that the 28 chapters composing the book have been grouped into the following main parts: sustainable materials and ecodesign aspects, composite materials and curing processes, modelling and testing, strength of adhesive joints, characterization and thermal behaviour, all of which provides an invaluable overview of this fascinating subject area. Results achieved from theoretical, numerical and experimental investigations can help designers, manufacturers and suppliers involved with high-tech composite materials to boost competitiveness and innovation productivity.

INTECH
open science | open minds

InTech Europe
University Campus STeP Ri
Slavka Krautzeka 83/A
51000 Rijeka, Croatia
Phone: +385 (51) 770 447
Fax: +385 (51) 686 166
www.intechopen.com

InTech China
Unit 405, Office Block, Hotel Equatorial Shanghai
No.65, Yan An Road (West), Shanghai, 200040, China
中国上海市延安西路65号上海国际贵都大饭店办公楼405单元
Phone: +86-21-62489820
Fax: +86-21-62489821

IntechOpen